The intestinal circadian clock drives microbial rhythmicity to maintain gastrointestinal homeostasis

Marjolein Heddes[1, 2,†] , Baraa Altaha[1, 2, †], Yunhui Niu[1, 2], Sandra Reitmeier[1, 2], Karin Kleigrewe[3], Dirk Haller[1, 2,], Silke Kiessling [1,2,4,*]

*Corresponding Author: Dr. Silke Kiessling, silke.kiessling@tum.de

[†]These authors contributed equally

[1] ZIEL - Institute for Food & Health, Technical University of Munich, 85354 Freising, Germany

[2] Chair of Nutrition and Immunology, Technical University of Munich, Gregor-Mendel-Str. 2, 85354 Freising, Germany

[3] Bavarian Center for Biomolecular Mass Spectrometry, Technical University of Munich, Gregor-Mendel-Str. 4, 85354 Freising, Germany

[4] Faculty of Health and Biomedical Science, University of Surrey, Stagg Hill Campus, GU27XH, Guildford, UK

Summary

Diurnal (*i.e.*, 24-hour) oscillations of the gut microbiome have been described in various species including mice and humans. However, the driving force behind these rhythms remains less clear. In this study, we differentiate between endogenous and exogenous time cues driving microbial rhythms. Our results demonstrate that fecal microbial oscillations are maintained in mice kept in the absence of light, supporting a role of the host's circadian system rather than representing a diurnal response to environmental changes. Intestinal epithelial cell-specific ablation of the core clock gene *Bmal1* disrupts rhythmicity of microbiota. Targeted metabolomics functionally link intestinal clock-controlled bacteria to microbial-derived products, in particular branched-chain fatty acids and secondary bile acids. Microbiota transfer from intestinal clock-deficient mice into germ-free mice altered intestinal gene expression, enhanced lymphoid organ weights and suppressed immune cell recruitment. These results highlight the importance of functional intestinal clocks for circadian microbiota composition and function, which is required to balance the host's gastrointestinal homeostasis.

Introduction

Various physiological processes show 24-hour fluctuations. These rhythms are the expression of endogenous circadian (Lat. circa = about; dies = day) clocks that have evolved in most species [1] to facilitate anticipation of daily recurring environmental changes. In mammals, the circadian system includes a central pacemaker regulating sleep-wake behavior and orchestrating subordinated tissue clocks by humoral and neuronal pathways [2]. At the cellular level, these clocks consist of inter-regulated core clock genes [3] that drive tissue-specific transcriptional programs of clock-controlled genes (CCGs) [4]. Through these CCGs, circadian clocks regulate various aspects of physiology including metabolism, gastrointestinal transit

42 time (GITT), mucus secretion, antimicrobial peptide secretion, immune defense and intestinal
43 barrier function (reviewed by [5-8]).
44 In mice, 10-15 % of gut bacteria undergo diurnal oscillations in their abundance influenced by
45 meal timing, diet type and other environmental conditions [9-11]. Recently, we found similar
46 rhythms in microbiota composition and function in population-based human cohorts [12].
47 Although functionality of the host's circadian system impacts microbial rhythmicity [10,13,14], it
48 is unclear which tissue clocks contribute to this effect.
49 A balanced gut microbiome promotes health and microbial dysbiosis has been linked to
50 metabolic diseases, colorectal cancer and gastrointestinal inflammation [12,15-17]. Similar
51 pathological consequences are associated with circadian rhythm disruption (reviewed by [18-20]),
52 which also induces microbiota dysbiosis [10,11,13,14,21]. Consequently, we hypothesized that
53 circadian regulation of microbiota composition and function may contribute to the host's GI
54 health.
55 Here, we functionally dissect the circadian origin of microbiota oscillations in mice. We provide
56 evidence that intestinal epithelial cell (IEC) clocks generate the majority of gut microbial
57 rhythms and their metabolic products, particularly short-chain fatty acids (SCFAs) and bile
58 acids (BAs). Transfer of microbiota from IEC clock-deficient mice in germ-free (GF) wild type
59 hosts directly indicate the consequences of microbiota arrhythmicity on the gastrointestinal
60 homeostasis. Thus, we identify a mechanistic link between IEC clocks, gut bacteria rhythms
61 and their functions through transfer experiments, showing the importance of rhythmic
62 microbiota for host physiology.

63 ## Results

64 ### Rhythms in microbiota are generated endogenously by the circadian system

65 Diurnal rhythms in microbiota composition and function have been demonstrated in animal
66 models and in humans [9-12]. However, it has not been demonstrated whether these rhythms are a

response to rhythmic external cues (*Zeitgebers)*, such as the light-dark cycle, or are generated by endogenous clocks [22] and, thus, persist when the organism is placed in an environment devoid of timing cues. To address this question, we compared fecal microbiota rhythms of the same wild-type mice kept in a rhythmic 12-hour light/12-hour dark (LD) cycle and constant darkness (DD) for two weeks (**Fig. 1A**). Host-driven rhythmic factors, which might influence microbiota composition, such as locomotor activity, food intake as well as total GI transit time (GITT), did not differ between light conditions (**Suppl. Fig 1A-D**). 16S rRNA profiling of fecal samples revealed clustering based on sampling time points rather than light condition (**Fig. 1B, 1E**). Generalized UniFrac distances (GUniFrac) quantification to ZT1 identified rhythmicity in both light conditions (**Fig. 1C**). Importantly, 24-hour rhythms of species richness and Shannon effective number of species found in LD persisted in DD, supporting their circadian origin (**Fig. 1D**). Rhythms were also preserved in DD on phylum level with the two most dominant phyla Bacteroidetes and Firmicutes, oscillating in antiphase (**Fig. 1E, F)**. Although microbiota composition is commonly analyzed by relative abundance, rhythmicity of highly abundant taxa may mask oscillations of small microbial communities, as previously demonstrated in fecal samples collected in LD [13]. Therefore, using synthetic DNA spikes, we performed relative quantification of the copy number of 16S rRNA genes according to Tourlousee et al. [23], from here on referred to as 'quantitative analysis'. With both approaches, highly abundant phyla and families, including *Lachnospiraceae* and *Muribaculaceae*, showed comparable circadian rhythmicity in LD and DD (**Fig. 1F; Suppl. Fig. 1E)**. Few families, such as *Prevotellaceae* showed significant diurnal (LD), but no circadian (DD) rhythmicity, suggesting that their rhythms are regulated by the environmental LD cycle (**Suppl. Fig. 1E**). After removal of low-abundant taxa (mean relative abundance > 0.1%; prevalence > 10%), the remaining 580 zero-radius OTUs (zOTUs) displayed robust and comparable 24-hour oscillations in both light conditions, independent of the analysis (**Fig. 1G, H; Suppl. Fig. 1F-I**). The wide distribution of peak abundances, e.g., bacteria peaking during the day (mainly belonging to

93 *Muribaculaceae*) and during the night (*Lachnospiraceae*) (**Fig. 1G, H; Suppl. Fig. 1F-H**),
94 suggests that different microbial taxa dominate different daytimes. Importantly, more than 60%
95 of all identified zOTUs were found to significantly oscillate in LD and in DD (**Fig. 1G, H,**
96 **Suppl. Fig. 1F-H, Suppl. table 1-3)**, suggesting that their rhythmicity is generated by the
97 circadian system. Notably, comparable amounts of rhythmic zOTUs belong to the major phyla
98 Firmicutes and Bacteriodetes (**Suppl. Table 2**). Previous literature identified lower percentages
99 of microbial rhythmicity [9,10]. To assess this discrepancy we compared our results with the
100 previously published data set from Thaiss and colleagues [24]. Although the different methods to
101 assign taxonomic units, namely OTUs (97 % similarity strain assignment) in contrast to zOTUS
102 (100% similarity strain assignment) caused disparity between amounts of rhythmic
103 OTUs/zOTUs, the total abundance of rhythmic microbiota was comparable between both
104 studies (Heddes et al: 74 %, Thaiss et al: 83%, **Suppl. Fig. 1L. Suppl. Table 4**). Rhythmicity
105 of the majority of zOTUs (e.g. the genera *Alistipes*, *Oscillibacter* and *Fusimonas*) identified in
106 our study by relative analysis was further validated by quantitative analysis (73 % in LD, 58 %
107 in DD) **(Suppl. Fig. 1 I, J).** The diurnal rhythmicity found in ¾ of all zOTUs examined in LD
108 using JTK_CYCLE [25] is generated by the endogenous circadian system, since DODR analysis
109 [26 27]confirmed that more than 95% of zOTUs show similar rhythmicity in DD (e.g. the genera
110 *Eubacterium* and members of the family *Lachnospiraceae*) (**Fig. 1G**; **Suppl. Fig. 1K, Suppl.**
111 **Table 1, Suppl. Table 3)**.

112 Robust microbial rhythms despite the absence of rhythmic food intake behavior

113 Light and food are the main *Zeitgeber* for the central and peripheral clocks, respectively [2,28]. In
114 our study, external light conditions only mildly effected microbial rhythms (**Fig. 1**) and
115 previous research showed that rhythmic feeding time influences the phasing of microbiota
116 rhythmicity [10,11]. This prompted us to determine the dependency of bacterial oscillation on
117 rhythmic food intake behavior by investigating microbiota rhythmicity in the absence of both

118 *Zeitgeber* food and light. Therefore we collected feces from starved mice during the 2nd day in
119 DD (**Fig. 2A**). Although starvation altered microbial composition, clustering according to
120 collection time points was significant in both feeding conditions (**Fig. 2B, D**). Microbiota
121 diversity became arrhythmic in the absence of food (**Fig. 2C**). However, rhythms persisted in
122 the two dominant phyla, highly abundant families, including *Muribaculaceae* and
123 *Lachnospiraceae* and the majority of zOTUs (**Fig. 2E-H, Suppl. Table 1**). Of note, circadian
124 food intake behavior enhanced the amount of rhythmic zOTUs by 16% according to DODR
125 analysis on quantitative data (**Suppl. Table 3**). Nevertheless, circadian rhythms of highly
126 abundant microbial taxa belonging to *Muribaculaceae* and *Ruminococcaceae* maintained under
127 starving conditions in both relative and quantitative analysis (**Fig. 2 E-I**).

128 Together, these data show that although rhythms in gut bacteria are slightly influenced by
129 environmental light and food conditions, intrinsic factors are the dominant drivers of circadian
130 microbiota fluctuations.

131 The intestinal circadian clock controls microbiota composition and function

132 An important role of the host clock on diurnal microbiota fluctuation has previously been
133 suggested based on experiments on mice with clock dysfunction in all tissues under LD
134 conditions [10,13,14]. The GI tract represents an important interface for cross-talk between IECs,
135 bacteria and their metabolites [29] and thus might likely be involved in controlling microbiota
136 composition. To identify the circadian origin of microbial rhythmicity, we used mice with IEC-
137 specific deletion of the essential core clock gene *Bmal1* (*Bmal1*$^{IEC-/-}$). The rhythmic activity,
138 food intake behavior as well as GITT and stool weight of *Bmal1*$^{IEC-/-}$ mice did not differ from
139 control littermates, reflecting a functional central pacemaker (**Suppl. Fig. 2A-E**). Arrhythmic
140 core clock gene expression in the jejunum, cecum and proximal colon, in contrast to rhythms
141 in the liver, confirmed intestine-specific clock ablation in *Bmal1*$^{IEC-/-}$ mice (**Suppl. Fig. 2F**).
142 Rhythmic genes relevant for host-microbe crosstalk, in particular *Tlr2*, *Muc2*, *Nfil3* and *Hdac3*

143 [30-35] lost rhythmicity in *Bmal1*$^{IEC-/-}$ mice (**Suppl. Fig. 2G**). In line with this, microbiota
144 composition in DD and LD differed significantly between *Bmal1*$^{IEC-/-}$ mice and controls (p =
145 0.037 DD, p=0.018 LD) and circadian rhythmicity in community diversity (species richness)
146 observed in control mice was abolished in *Bmal1*$^{IEC-/-}$ mice (**Fig. 3A, B, Fig. 4A**). Quantitative
147 analysis revealed loss of rhythmicity of Firmicutes in *Bmal1*$^{IEC-/-}$ mice in LD and DD (LD p= ,
148 DD p = 0.313), although, oscillation in relative abundance of the major phyla was found in both
149 genotypes, (**Fig. 3C, Fig. 4C**). Alterations in quantitative compared to relative rhythmicity
150 analyses are not due to differences in 16s copy number over time, as both genotypes show
151 similar patterns in LD and DD conditions (**Suppl. Fig. 2H, Fig. 4B**). In accordance to results
152 obtained from whole-body clock-deficient mice [13], IEC-specific loss of *Bmal1* decreased the
153 quantitative abundance of both phyla, which was not visible in relative data sets (**Fig. 3C, Fig.
154 4C**). Similarly, rhythmicity observed in the relative abundance of families, including
155 *Lachnospiraceae* and *Ruminococcaceae*, was abolished performing quantitative analysis
156 (**Suppl. Fig. 2I).** Furthermore, dramatically disrupted circadian oscillations of *Bmal1*$^{IEC-/-}$ mice
157 in both relative and quantitative analyses was observed on the level of all 580 identified zOTUs
158 illustrated by heatmaps (**Fig. 3D, E**). Of note, in *Bmal1*$^{IEC-/-}$ mice the phase of remaining
159 microbial oscillations was delayed using quantitative analysis (**Fig. 3D, E)**. Based on both
160 analyses more than 60 % of fecal zOTUs, which account for more than two-third of bacterial
161 abundance, underwent circadian oscillation in controls (**Fig. 3D, E, Suppl. Table 1)**.
162 Importantly, the amount of rhythmic zOTUs was dramatically reduced by ⅔ in mice with IEC-
163 specific *Bmal1* deficiency in both analyses, independent of the light conditions (**Fig. 3D, E,
164 Fig. 4D, I, Suppl. Table 1-3**. Circadian zOTUs in control mice, which were arrhythmic in
165 *Bmal1*$^{IEC-/-}$ mice in both relative and quantitative analysis, belong predominantly to the families
166 *Lachnospiraceae* and *Ruminococcaceae* of the phylum Firmicutes **(Suppl. Fig. 3J, Suppl.
167 Table 2).** The genera *Lactobacillus, Ruminococcus, Anaerotignum, Odoribacter* and *Alistipes*
168 are among the taxa with differential rhythmicity comparing *Bmal1*$^{IEC-/-}$ mice with their controls

169 based on DODR analysis and in addition significantly differed in their abundance between
170 genotypes (**Fig. 3F, G**). Although the majority of zOTUs was under intestinal clock control,
171 rhythmicity of around 20% of zOTUs (e.g. *Lactobacillus animalis* and *Pseudoflavonifractor*)
172 persisted in *Bmal1*$^{IEC-/-}$ mice (**Fig. 3D, E, Suppl. Table 1**). To address whether these remaining
173 rhythms were driven by the rhythmic food intake behavior observed in *Bmal1*$^{IEC-/-}$ mice kept
174 under ad libitum conditions in DD (**Suppl. Fig. 2D**), microbiota rhythmicity in *Bmal1*$^{IEC-/-}$ mice
175 was analyzed in feces from starved mice during the 2nd day in DD (**Fig. 2A**). Although beta
176 diversity was significantly altered in the absence of rhythmic food intake profiles of major phyla
177 were undistinguishable between feeding conditions **(Fig. 4E, F).** Only a small amount of the
178 remaining rhythmic zOTUs in *Bmal1*$^{IEC-/-}$ mice significantly lost rhythmicity upon starvation
179 based on DODR analysis **(Suppl. Table 3)**, such as bacteria belonging to *Turicimonas muris*
180 and *Muribaculaceae,* and (**Fig. 4G-I, Suppl. Table 1).**

181 Taken together, rhythmicity analyses of zOTU in *Bmal1*$^{IEC-/-}$ mice and controls under different
182 light and food conditions **(Fig. 3, Fig. 4, Suppl. Fig. 2**) highlight that the IEC clock represent
183 the dominant driver of circadian gut microbiota oscillation.

184 Intestinal clock-controlled microbial functions balance gastrointestinal homeostasis.

185 To address the potential physiological relevance of microbial oscillations, PICRUST 2.0
186 analysis was performed on intestinal-clock controlled zOTUs. Loss of microbial rhythmicity in
187 *Bmal1*$^{IEC-/-}$ mice was reflected in assigned pathways involved in sugar- and amino acid
188 metabolism, vitamin biosynthesis and relevant for fatty acid (FA) metabolism such as β-
189 oxidation, FA elongation and short-chain FA (SCFA) fermentation (**Fig 5A, Suppl. Fig 3 I**).
190 This prompted us to test the functional connection between intestinal clock-driven microbial
191 rhythmicity and intestinal homeostasis (**Fig. 5B-H**). Indeed, Procrustes analyses (PA) identified
192 an association between intestinal clock-controlled zOTUs and SCFA concentrations measured
193 by targeted metabolomics ($p = 0.001$) (**Fig. 5B**). The level of valeric acid ($p = 0.04$, Mann-

194 Whitney U test) and low-abundant branched-chain fatty acids (BCFAs) (p = 0.01, Mann-
195 Whitney U test), including isovaleric, isobutyric, 2-methylbutyric differed between genotypes,
196 although the amount of total and highly abundant SCFAs were comparable (**Fig 5C, Suppl.**
197 **Fig. 3A**). Nevertheless, concentrations of SCFAs negatively correlated with the relative
198 abundance of intestinal clock-driven taxa, mainly belonging to the family *Muribaculaceae* of
199 the phylum Bacteroidetes (**Fig. 5D, Suppl. Fig. 3B**). Positive significant correlations with
200 multiple SCFAs, in particular BCFAs, where found with zOTUs belonging to the phylum
201 Firmicutes, including the SCFA producers *Lachnospiraceae* and *Ruminococcaceae* (**Suppl.**
202 **Fig. 3B**) [36]. Similar to the results observed for SCFAs, associations were found between
203 intestinal clock-controlled zOTUs and BAs levels (p = 0.04, **Fig. 5G**). Positive correlations
204 with primary BAs and negative correlations with secondary BAs were observed with several
205 intestinal clock-controlled taxonomic members mainly belonging to Firmicutes (**Fig. 5D,**
206 **Suppl. Fig. 3D**). For example, DHLCA and 7-sulfo-CA negatively correlated with
207 *Oscillibacter* and *Eubacterium* (**Fig. 5D, Suppl. Fig. 3D**). In addition, almost half of the
208 measured BAs differed among genotypes and, BAs, such as the conjugated primary BA, TCDA,
209 and secondary BA, 7-sulfo-CA, lost rhythmicity in Bmal1$^{IEC-/-}$ mice (**Fig. 5E-F**). Interestingly,
210 most alterations were observed for secondary BAs (**Fig. 5H, Suppl. Fig3 C**), which were linked
211 to various GI diseases (reviewed by [37]). In summary, these results indicate that deletion of
212 intestinal clock function causes loss of rhythmicity in the majority of bacterial taxa and alters
213 microbial functionality.

214 Transfer of arrhythmic intestinal clock-controlled microbiota disturbs GI homeostasis

215 To further test the physiological relevance of intestinal clock-driven rhythmic microbial
216 composition and its functionality on host physiology, GF C57BL/6 mice were colonized with
217 cecal content from *Bmal1$^{IEC-/-}$* or control mice (n=4) (**Fig. 6A**). Importantly, ~76 % of bacteria
218 from the control and *Bmal1$^{IEC-/-}$* donor, were transferred into the recipients (**Suppl. Fig. 3E**).

219 Reduced richness was observed in mice after microbiota transfer (**Suppl. Fig. 3F**), in line with
220 previous reports [38]. Interestingly, microbiota composition of recipient wild-type hosts
221 significantly differed depending on the genotype of the donor (**Fig. 6B; Suppl. Fig. 3G,H**).
222 Most of the transferred taxa belonged to Firmicutes, whose rhythmicity strongly depends on a
223 functional intestinal clock, whereas abundances in Bacteroidetes were highly suppressed (**Fig.**
224 **6C; Suppl. Fig. 3G**). Importantly, lack of rhythmicity was transferred to mice receiving
225 microbiota from *Bmal1*$^{IEC-/-}$ mice (**Fig. 6D, E**). In particular rhythmicity of zOTUs belonging
226 to e.g. *Alistipes*, shown to be driven by the gut clock (**Fig. 3F**) and maintained circadian
227 rhythmicity in the host after transfer from control donors, lack rhythmicity in mice receiving
228 microbiota from *Bmal1*$^{IEC-/-}$ mice (**Fig. 6E**). Interestingly, after transfer of *Bmal1*$^{IEC-/-}$ -
229 associated arrhythmic microbiota several bacterial-derived metabolites, including BCFA as
230 well as the secondary bile ketolitocholic acids were significantly upregulated and the primary
231 BA β-muricholic acid (b-MCA) was significantly downregulated **(Fig. 6F)**, similar to
232 observations in made in donor mice **(Fig 5C,F, Suppl. Fig. 3A-D).** Moreover, altered
233 expression of intestinal clock genes in jejunum and colon was observed after transfer of
234 arrhythmic microbiota in comparison to recipient mice receiving rhythmic microbiota (**Suppl.**
235 **Fig. 4A**). In addition the expression of genes involved in host-microbe interaction, including
236 *Arg2* and *Tlr4,* significantly differed depending on the genotype of the donor (**Fig. 6G**).
237 Arrhythmic microbiota transfer induced the expression of *Il33 and NfkB* both known to be
238 involved in intestinal inflammatory responses [39,40] and reduced the expression of *Ang4* and
239 *Hdac3* (**Fig. 6G**), which are known to integrate microbial and circadian cues relevant for
240 inflammatory and metabolic intestinal functions [33,41,42,31,35]. Although mesenteric lymph nodes
241 and colon weights of mice associated with arrhythmic microbiota were undistinguishable from
242 controls, and histology scores were unaffected, we noticed an increase in spleen and jejunum
243 weight (**Fig. 6H, Suppl. Fig. 4B, C**), indicating a role of microbial rhythmicity on host
244 intestinal homeostasis. Indeed, transfer of arrhythmic microbiota altered immune cell

245 recruitment to the lamina propria. For example, an increase in dendritic cells (CD11c+) was
246 detected in the small intestine whereas recruitment of T cells (CD3+CD4+, CD3+CD8+) and
247 dendritic cells (CD11c+) to the lamina propria of the colon was decreased (**Fig. 6I, Suppl. Fig.**
248 **4D**). Similar trends in immune cell recruitment and intestinal gene expression were observed
249 in *Bmal1*$^{IEC-/-}$ mice in SPF conditions **(Suppl. Fig. 4E, F),** suggesting that intestinal-clock
250 controlled microbes influence gut immune homeostasis. Importantly, alterations found
251 following transfer of *Bmal1*$^{IEC-/-}$ -associated arrhythmic microbiota were not observed after
252 transfer of microbiota from control mice kept in either LD, DD or starvation conditions,
253 highlighting the physiological relevance of gut-clock-controlled microbiota **(Suppl. Fig. 4G-**
254 **I).**

255 Together, these results indicate that deletion of intestinal clock function caused loss of
256 rhythmicity in the majority of bacterial taxa, alters microbial functionality and resets the host's
257 intestinal homeostasis.

258

259 ## Discussion

260 Diurnal microbial oscillations in the major phyla and families have previously been
261 demonstrated in humans and mice by us and others [9-13]. Here we provide evidence that
262 rhythmicity of the majority of these taxa persists even in the absence of external timing cues,
263 demonstrating the endogenous origin of fecal bacterial circadian rhythms. In contrast, strongly
264 attenuated microbial rhythms in cecal and ileal content were found in mice kept in DD [43].
265 Differences in the amount and type of oscillating microbes between studies may be explained
266 by variations in microbiota composition of the mouse lines, microbial ecosystem between
267 facilities and niches within the GI tract. Moreover, our comparison analysis indicates that the
268 discrepancy in total amounts of oscillating taxa between our study and previous studies[9,10] is
269 likely due to the different methods used to classify groups of closely related taxa. The

270 comparability between studies may additionally be impacted by methodological differences,
271 such as differences in the 16S rRNA variable target gene region used for amplicon sequencing
272 (here: V3-V4, [43]: V4, [10]: V1-V2, [21].: V1-V3, [44]: Metatranscriptome) as well as the sampling
273 intervals (here: 3h/day, [43]: 6h/day, [10]: 4h/day).

274 Our results obtained from constant environmental conditions suggest that circadian microbiota
275 regulation is primarily rooted in host or bacterial intrinsic circadian mechanisms. Indeed, using
276 IEC-specific *Bmal1*-deficient mice, we provide the first demonstration for a dominant role of
277 intestinal clocks in driving circadian microbiota composition. Lack of *Bmal1* in IECs led to
278 dramatic loss of microbiota rhythmicity, predominantly belonging to the phylum Firmicutes,
279 which was independent of whether relative or quantitative analyses was used. Of note, both
280 microbiota analyses in this study did not always yield identical results, highlighting the
281 importance of both analyses to interpret circadian microbiota composition. Microbiota
282 composition is commonly analyzed by relative abundance; yet this analysis may exaggerate
283 microbial rhythmicity due to masking by highly abundant taxa [13]. Arrhythmicity in taxa (e.g.
284 *Lactobacillaceae, Odoribacteraceae* and *Lachnospiraceae)* was previously documented in
285 mice lacking *Bmal1* or *Per1/2* tissues-wide [10,13]. Loss of oscillations of the same taxa among
286 others was observed in $Bmal1^{IEC-/-}$ mice, identifying the IEC-clock to generate rhythmicity of
287 these bacteria. This prominent role of the intestinal clock in driving microbial rhythmicity was
288 further validate on data obtained in LD condition. Few of the remaining bacteria which were
289 unaffected by IEC clock-deficiency, lost circadian rhythmicity upon starvation. Some of these
290 taxa have previously been reported to be influenced by food availability [11]. A prominent role
291 for the timing of food intake on microbial rhythmicity was frequently suggested [9-11]. However,
292 we demonstrate that even in the absence of food, rhythmicity of dominant bacteria persisted,
293 thus rhythmic food intake is not required to drive microbiota oscillations. Accordingly, in mice
294 supplied with constant intravenous parenteral nutrition cecal microbiota composition oscillated

295 [9]. Importantly, the majority of microbial rhythms was abolished in *Bmal1*$^{IEC-/-}$ mice even though
296 these mice show rhythmic food intake behavior. These results further highlight that IEC clocks
297 are the dominant driver whereas environmental changes as well as food-intake are mere
298 modulators of microbial rhythms.

299 Mechanisms how intestinal clocks regulate microbiota rhythms likely involve local epithelial-
300 microbe interactions and immune functions, including pattern recognition receptors, such as
301 Toll-Like Receptors (TLRs), Aryl hydrocarbon receptors and nuclear receptors as well as
302 antimicrobial peptide production and mucus secretion, all previously found to oscillate
303 diurnally [32,33,46]. Accordingly, we found IEC clocks to be essential for rhythmic expression of
304 related genes, such as *Tlr2*, *Ang4*, *Muc2*, *Nfil3* and *Hdac3,* which are engaged in bidirectional
305 microbe-host communication. For example, IEC-specific deletion of *Hdac3* or loss of *Tlr2*
306 altered microbial composition and influenced intestinal homeostasis [47,48]. Furthermore, *Muc2*
307 can affect microbiota composition by allowing bacteria to metabolize mucin glycans [49], which
308 through cross-feeding affects the abundance of other microbial taxa [50]. However, future studies
309 are required to functionally investigate intestinal clock mechanism controlling microbiota
310 composition.

311 Circadian disruption due to life style has been correlated to microbiota dysbiosis and human
312 health (reviewed by [51]). Recently, we found a functional link between arrhythmicity of
313 microbiota and the development of obesity and T2D [12]. Here we demonstrate intestinal-clock
314 dependent rhythmicity of taxa involved in SCFA fermentation, such as *Lachnospiraceae,*
315 *Ruminococcaceae* and *Odoribacteraceae*, lactate acid producing bacteria e.g.
316 *Lactobacillaceae*, mucus foragers, such as *Muribaculaceae, Rickenellaceae* and
317 *Lachnospiraceae* [36,52,53]. Moreover, taxa capable to convert bile acids (BAs), including
318 *Lactobacillus* and *Ruminococcus* [54] are regulated by intestinal circadian clocks. Consequently,
319 IEC clocks likely influence microbiota function. Indeed, functional analysis based on 16S

320 rRNA gene data revealed pathways such as SCFA fermentation, amino-acid and carbohydrate
321 metabolism are associated to intestinal clock-controlled taxa. Many among the identified
322 pathways were shown to diurnally oscillate in healthy individuals, to lose rhythmicity in clock
323 deficient mice, and are associated with host's health [10,12,55]. Targeted metabolite analysis further
324 confirmed that arrhythmicity in intestinal clock-controlled taxa is reflected in alterations of key
325 metabolites involved in lipid signaling pathways such as SCFAs and BAs. Both of these
326 microbiota-related metabolites are known to diurnally oscillate and impact, among others host
327 immune and metabolic functioning [9,56-60]. Notably, high levels of secondary BAs, e.g. DCAs
328 and HDCAs identified in *Bmal1*$^{IEC-/-}$ mice, were also found in subjects with metabolic disorders
329 including obesity and T2D [61-64]. Moreover, TUDCA lost circadian rhythmicity in *Bmal1*$^{IEC-/-}$
330 mice and was found to ameliorate insulin sensitivity in both obese mice and humans [65,66]. In
331 addition, accumulation of BAs within the host has been associated with several GI diseases.
332 For example, increased levels of the sec. BA DCA and taurine-conjugated BAs were linked to
333 colorectal cancer in mice (reviewed by Jia and colleagues [67]). These results support the
334 hypothesis that a functional intestinal clock balances GI health by driving microbial function.

335 Transfer experiments provide direct evidence for the physiological relevance of intestinal
336 clock-controlled microbiota and their functions. Microbial rhythmicity and arrhythmicity
337 depending on the donor genotype induced molecular and physiological changes in the healthy
338 hosts. Notably, a functional intestinal clock in recipients seems to require longer than 5 weeks
339 to restore microbial rhythmicity, suggesting strong microbe-host clock interactions. Indeed, this
340 was supported by altered clock gene expression in recipients receiving arrhythmic microbiota
341 and is in accordance with a report indicating a role of microbial rhythmicity in programing host
342 transcriptome rhythmicity [24]. Additionally, the alteration of microbial metabolite production in
343 recipients, which reflect the results obtained from donor mice, e.g. upregulated BCFAs and sec.
344 BAs. may have influenced intestinal clock functions, since a direct impact on rhythmicity in

345 intestinal epithelial cells and subsequent metabolic responses in the host has been provided
346 previously [9,49].

347 Transfer of arrhythmic microbiota from intestinal clock-deficient mice altered several genes
348 involved in inflammation, antimicrobial peptide production and intestinal epithelial functioning
349 including *Tnf-α, Tlr2, Lgr5, Ffar2, Hdac3* and *Nf-kB* [39-41,68-71]. Changes in the expression of
350 these genes due to reception of arrhythmic microbiota might have caused the observed immune
351 phenotype in recipients. For example, *Tlr2* senses the presence of microbe-associated molecular
352 patterns and is capable to regulate the host's immune system against pathogenic infiltration by
353 regulating *Tnf-α* cytokine production of CD8+ T-cells [72,73]. Moreover, *Hdac3* and *Il33* also
354 plays an important role in microbe-host crosstalk [47,74]. Mouse models lacking HDAC3 show
355 high susceptibility to DSS-induced inflammation, partly by activation of NF-kb, the latter also
356 observed in our mouse model [47,75] . Consequently, altered regulation of *Tlr2*, *Tnf-α, Hdac3*, and
357 *IL-33* expression observed in mice receiving arrhythmic microbiota, likely disturbed
358 gastrointestinal homeostasis. Indeed, enhanced lymphoid tissues weight and suppressed
359 recruitment of T-cell and dendritic cell populations to the lamina propria within the colon was
360 found in GF mice receiving arrhythmic microbiota from intestinal clock-deficient mice.
361 Immune cell recruitment represents an important aspect in the gastrointestinal immune defense
362 (reviewed by [76]). Interestingly, we observed similar alterations and microbial-derived
363 metabolite changes in recipients and SPF donors, indicating that microbiota might transfer the
364 phenotype from the donor to recipients. Discrepancies between the immune phenotype
365 observed in donor and recipient mice might be caused by genetic loss of Bmal1 in the intestine
366 of donors and feedback from arrhythmic microbiota on intestinal tissue of rhythmic recipients.
367 In contrast, transfer of microbiota from control mice kept in LD, DD or in starving conditions
368 did not cause the same alterations in immune cell recruitment, gene expression or microbial
369 metabolites levels. These results provide the first evidence that intestinal clock-controlled

370 rhythmic gut bacteria are crucial for a balanced intestinal immune homeostasis, and likely
371 influence the immune response to pathogens, infection and inflammation.

372 Taken together, a functional intestinal clock represents a key element to maintain
373 gastrointestinal health by driving rhythmicity of gut bacteria and microbial products. Since
374 intestinal clock functions effect bacterial taxa required for a balanced immune defense, it
375 remains to be studied whether arrhythmicity of intestinal clock-controlled taxa is causal for the
376 development of gastrointestinal diseases. In the scope of previous associations of arrhythmic
377 microbiota and their products with T2D and IBD [12,77], our data highlight the relevance to further
378 investigate intestinal clock mechanisms driving bacterial rhythmicity for human health.

ADDITIONAL INFORMATION (CONTAINING SUPPLEMENTARY INFORMATION LINE (IF ANY) AND CORRESPONDING AUTHOR LINE)

ACKNOWLEDGEMENT

The Technical University of Munich provided funding for the ZIEL Institute for Food & Health, animal facility support, technical assistance and support for 16S rRNA gene amplicon sequencing. Johanna Bruder provided assistance with animal experiments and preliminary data collection.

AUTHOR CONTRIBUTIONS

SK conceived and coordinated the project. MH, BA performed mouse experiments and fecal samples collection. BA, MH and YN provided tissue samples and performed gene expression analysis. SK and MH analyzed activity and food intake behavior. MH, BA, SR and SK performed 16S rRNA gene sequencing and bioinformatics analysis. BA and MH analyzed predicted microbial functionality. YN performed FACS analyses. MH and KK performed targeted metabolomics and data analysis. SK supervised the work and data analysis. SK and DH secured funding. MH, BA, DH and SK wrote the manuscript. All authors reviewed and revised the manuscript. MH and BA contributed equally to this work.

FUNDING

SK was supported by the German Research Foundation (DFG, project KI 19581) and the European Crohn´s and Colitis Organisation (ECCO, grant 5280024). SK and DH received funding by the Funded by the Deutsche Forschungsgemeinschaft (DFG, German Research Foundation) – Projektnummer 395357507 – SFB 1371).

402 ## MATERIALS & CORRESPONDENCE

403 Correspondence to Dr. Silke Kiessling, Chair of Nutrition and Immunology, Technical
404 University of Munich, Gregor-Mendel-Str. 2, 85354 Freising, Germany.

405 ## DECLARATION OF INTEREST

406 The authors declare no competing interests.

---

407 **METHODS**

408 *Ethics Statement*

409 Experiments were conducted at Technical University of Munich in accordance with Bavarian
410 Animal Care and Use Committee (TVA ROB-55.2Vet-2532.Vet_02-18-14).

411 *Mouse models*

412 *Bmal1$^{IEC\ tg/wt}$ and Bmal1$^{IECfl/fl}$ mouse generation*

413 Male epithelial intestinal epithelial cell-specific *Bmal1* knock-out *(Bmal1fl/fl* x Villin CRE/wt;
414 referred to as *Bmal1$^{IEC-/-}$*) mice and their control littermates (*Bmal1fl/fl* x Villin wt/wt ; referred
415 to as *Bmal1$^{fl/fl}$*) on a genetic C57BL/6J background were generated as previously described [78].
416 Breeding was performed by crossing *Bmal1fl/fl* x Villin CRE/wt with *Bmal1fl/fl* x Villin wt/wt.
417 Unless otherwise stated, mice were kept in LD 12:12 cycles (300 lux), with lights turned on at
418 5am (*Zeitgeber* time (ZT0) to 5pm (ZT12)). All mice were single housed at the age of 8 weeks
419 in running wheel-equipped cages with ad libitum access to chow and water and under specific-
420 pathogen free (SPF) conditions according the FELASA recommendation. In order to minimize
421 cage-related bias in microbiota composition [79], littermates and litters of comparable age from
422 as few as possible breeding pairs and cages were selected.

423 *Behavior analysis*

424 All male mice, unless stated otherwise, were individually housed in cages with running wheels.
425 Handling and activity measurements during experiments were performed as described [80].
426 Wheel-running activity was analyzed using ClockLab software (Actimetrics). The last 10-14
427 days of each condition were used to determine the period (tau, calculated using a X^2
428 periodogram and confirmed by fitting a line to the onsets of activity), the duration of the active
429 period (alpha), the amount of activity and the subjective day/night activity ratio (where the
430 subjective day under DD conditions is the inactive period between the offset of activity and the

431 onset of activity and the subjective night is the active period between the onset of activity and
432 the offset of activity).

433 *Light-dark (LD) and constant darkness (DD) conditions and fecal sample collection*

434 Male *Bmal1*$^{IEC-/-}$ and their control littermates *Bmal1*$^{IECfl/fl}$ were maintained under LD cycle for
435 2 weeks (age 8-10 weeks), switched to a DD cycle for 2 more weeks (age 10-12 weeks), kept
436 in constant light (LL) for an additional 2 weeks (age 12-14w) and finally returned back to LD
437 till the age of 18-20 weeks before sacrifice. Average daily food intake was measured over 5
438 consecutive days in the second week of the above indicated light conditions. Of note, Fecal
439 sample collection in darkness was performed after adjusting for each mouse's individual free-
440 running period (**Suppl. Fig. 2A**). For example, the activity period varied by ~0.5 hours per day
441 within mice of the same genotype and consequently accumulates to a ~7 hour phase difference
442 between individual mice after 2 weeks in DD. Fecal collection in LD was performed according
443 to normal *Zeitgeber* time. Samples were collected every 3 hours over the course of a 24h-day
444 (**Fig. 1A, Suppl. Fig. 2A**).

445 *Food deprivation*

446 11-week-old *Bmal1*$^{IEC-/-}$ and control male mice with *ad libitum* food intake were used for fecal
447 sample collection. At the age of 12-13 weeks control littermates from *Bmal1*$^{IEC-/-}$ mice were
448 starved beginning at CT1 on the 1st day in DD. Fecal samples were collected as detailed above
449 starting at CT13 on the 2nd day in DD (after 13 hours of starvation) till CT10 (after 34 hours of
450 starvation) at the indicated time points (**Fig. 2A**).

451 *Food intake pattern and analysis*

452 The diurnal food intake pattern of individually housed mice was recorded using an automated
453 monitoring system (TSE LabMaster Home Cage Activity, Bad Homburg, Germany) at the age
454 of 10-12 weeks. Mice were habilitated for 3 days. Then data were collected for a full 24-hours
455 profile at the 4th day. Cumulative food intake was recorded through high precision balances

456 connected to the food baskets. Food basket weight were summed up in 1 min intervals. Total
457 food intake was calculated as 1st derivative of cumulative food intake and consumption was
458 summed up at intervals of 1 hour. One-minute intervals where the weight loss was directly
459 followed by a similar weight gain in food baskets within a period of 3 minutes were excluded.
460 Circadian food intake of individually housed mice was recorded in the second day of darkness
461 by weighing the food every 3 hours.

462 *Complete gastrointestinal transit time*

463 Complete GI transit time (GITT) was measured by administering natural carmine red (6%,
464 SigmaAldrich) dissolved in 0.5% methylcellulose (Sigma-Aldrich) by gavage (100ul)
465 according to [81]. 16-18 week-old male *Bmal1*$^{IEC-/-}$ and *Bmal1*$^{fl/fl}$ mice were starved 6h prior to
466 gavage. Time of gavage was considered T0. In case of presence, fecal pellets were taken out of
467 the cage every 10 minutes and checked for red color. GITT was registered as the time between
468 T0 and the time of presence of carmine red in the fecal pellets.

469 *Tissue collection in SPF conditions*

470 All animals were sacrificed by cervical dislocation at the age of 18-20 weeks in the second day
471 of darkness at the indicated circadian times (CT) or in LD12:12 conditions, in 4 hour intervals
472 starting at 1 hour after lights off (ZT1). In constant darkness samples were collected at the
473 indicated time points used for control mice in LD. Eyes were removed prior to tissue dissection.
474 Tissues were harvested and snap frozen on dry ice and stored in -80 degrees.

475

476 *Gene expression analysis (qRT-PCR) Quantitative real-time PCR*

477 RNA was extracted from snap frozen tissue samples with Trizol reagent. cDNA was
478 synthesized from 1000ng RNA using cDNA synthesis kit Multiscribe RT (Thermofischer
479 Scientific). qPCR was performed in a Light Cylcer 480 system (Roche Diagnostiscs,

480 Mannheim, Germany) using Universal Probe Library system according to manufacturer's
481 instructions. For genes expression the following primers and probes were used: Brain and
482 Muscle ARNT-Like 1 *(Bmal1)* F 5'-ATTCCAGGGGGAACCAGA-' R 5'-
483 GGCGATGACCCTCTTATCC-3' Probe 15, Period 2 *(Per2)* F 5'-
484 TCCGAGTATATCGTGAAGAACG-3' R 5'- CAGGATCTTCCCAGAAACCA-3' probe 5,
485 Nuclear receptor subfamily 1 group D member 1 *(Reverbα)* F 5'-
486 AGGAGCTGGGCCTATTCAC-3' R 5'-CGGTTCTTCAGCACCAGAG-3' probe 1, Toll-like
487 receptor 2 *(Tlr2)* F- 5'-GGGGCTTCACTTCTCTGCTT-3' R 5'-AGCA
488 TCCTCTGAGATTTGACG-3' probe 50, Angiogenin 4 *(Ang4)* F 5'-
489 CCCCAGTTGGAGGAAAGC-3' R 5'-CGTAGGAATTTTTCGTACCTTTCA-3' probe 106,
490 Mucin 2 *(Muc2)* F 5'- GGCAGTACAAG AACCGGAGt-3' R 5'-
491 GGTCTGGCAGTCCTCGAA-3' probe 66, Histone Deacetylase 3 *(Hdac3)* F 5'- GAGAGGTC
492 CCGAGGAGAAC-3' R 5'-CGCCATCATAGAACTCATTGG-3' probe 40, Tumor necrosis
493 factor alpha *(Tnfa)* F 5'- TGCCTATGTCTCAGCCTCTTC-3' R 5'-
494 GAGGCCATTTGGGAACTTCT-3' probe 49, Leucine Rich Repeat Containing G Protein-
495 Coupled Receptor 5 *(Lgr5)* F 5'- CTTCACTCGGTGCAGTGCT-3' R 5'-
496 CAGCCAGCTACCAAATAGGTG-3' probe 60, Toll like receptor 4 *(Tlr4)* F 5'-
497 GGACTCTGATCATGGCACTG -3' R 5'-CTGATCCATGCATTGGTAGGT-3' probe 2,
498 Nuclear factor kappa-light-chain-enhancer of activated B cells *(Nfkb)* F 5'-
499 CCCAGACCGCAGTATCCAT -3' R 5'- GCTCCAGGTCTCGCTTCTT-3' probe 47. RNA
500 abundance was normalized to the housekeeping gene Elongation factor 1-alpha *(Ef1a)* F 5'-
501 GCCAAT TTCTGGTTGGAATG-3' R 5'-GGTGACTTTCCATCCCTTGA-3' probe 67. For
502 Interleukin33 (*Il33*) gene was used syber green to run the gene using the following primer F 5'-
503 GAACATGAGTCCCATCAAAG -3' R 5'- CAGCTGGTTATCTTTTACTCC -3' and RNA
504 abundance was normalized to the housekeeping gene *Ef1a* F 5'- GCCAAT
505 TTCTGGTTGGAATG-3' R 5'-GGTGACTTTCCATCCCTTGA-3'.

506 *High-Throughput 16S Ribosomal RNA (rRNA) Gene Amplicon Sequencing Analysis*

507 Genomic DNA was isolated from snap-frozen fecal pellets according to a modified protocol of
508 Godon and colleagues [82], as previously described [12]. DNA NucleoSpin gDNA columns
509 (Machery-Nagel, No. 740230.250) were used for DNA purification. In a two-step PCR the V3-
510 V4 region (using the primers 341F-ovh and 785r-ov) of the 16S rRNA gene was amplified from
511 24 ng DNA. After pooling, the multiplexed samples were sequenced on an Illumina HiSeq in
512 paired-end mode (2x250 bp) using the Rapid v2 chemistry, in accordance with [12]. Two negative
513 controls, consisting of DNA stabilizer without stool, were used for every 45 samples to control
514 for artifacts and insure reproducibility. High-Quality sequences of read counts > 5000 were
515 used for 16s rRNA data analysis. Reads FASTQ files were consequently processed using an in-
516 house developed NGSToolkit (Version Toolkit 3.5.2_64) based on USEARCH 11 [83]. A trim
517 score of 5 was used on the 5' end and 3'end for the R1 and R2 read followed by chimera removal
518 [84] using the FASTQ mergepair script of USEARCH [83]. Quality filtered reads were merged,
519 deduplicated, clustered and a denoised clustering approach was applied to generate zero-radius
520 operational taxonomic units (zOTUs) [83,85]. Using zOTUs analysis provide the best possible
521 resolution considering the 16s rRNA sequencing, by correcting the sequencing error (denoising
522 step) and then identifying each unique sequence (100% similarity) as a different microbial
523 strain. On the other hand, previously OTU analysis was used, which is based on merging
524 different strains which has more than 97% similarity into one single OTU, and assign it to one
525 microbial strain[45]. Taxonomic assignment was performed with the EZBiocloud database[86].
526 Notably, For Suppl. Fig 1L Taxa were assigned to Greengenes database in order to be able to
527 compare our results with the data obtained in the study by Thaiss and colleagues [10]. Data was
528 further analyzed with the R-based pipeline RHEA [87]. Phylogenetic trees are generated by a
529 maximum likelihood approach, which was performed on an alignment generated by MUSCLE
530 with the software MegaX [88]. Trees were visualized and annotated with the use of the online tool
531 EvolView (http://www.evolgenius.info/evolview/) [89]. Spike-in of 12 artificial DNA standards

532 mimicking 16S rRNA genes (a surrogate for bacterial numbers) were used to determine the
533 quantitative copy numbers of rRNA genes per gram of fecal sample between samples. Briefly,
534 the same amount of artificial DNA (6ng) was added to each weighted fecal sample before DNA
535 extraction. After sequencing as described above, FASTQ files were mapped against the spike
536 FASTA sequences (using bowtie2), removing the spike reads and generating a new FASTQ
537 file. By comparing the spike sequencing reads to the fecal bacterial reads; we calculate the
538 quantitative number of 16S rRNA gene copies per gram of sample. The copy number of 16S
539 rRNA gene is proportional to the number of bacteria present in a sample. Thus, this approach
540 enables estimation of microbial abundances relative between samples, suitable for comparative
541 analysis according to Tourlousse et al. 2017 [23].

542 *Targeted metabolite analyses*

543 *Sample preparation for targeted metabolite analyses*

544 Approximately 20 mg of mouse fecal pellet was weighed in a 2 mL bead beater tube (CKMix
545 2 mL, Bertin Technologies, Montigny-le-Bretonneux, France) filled with 2.8 mm ceramic
546 beads. 1 mL of methanol-based dehydrocholic acid extraction solvent (c=1.3 µmol/L) was
547 added as an internal standard for work-up losses. Fecal samples were extracted with a bead
548 beater (Precellys Evolution, Bertin Technolgies) supplied with a Cryolys cooling module 3
549 times each for 20 seconds with 15 seconds breaks in between at 10.000 rpm.

550 *Targeted bile acid measurement*

551 20 µL of isotopically labelled bile acids (ca. 7 µM each) were added to 100 µL of sample
552 extract. Targeted bile acid measurement was performed using a QTRAP 5500 triple quadrupole
553 mass spectrometer (Sciex, Darmstadt, Germany) coupled to an ExionLC AD (Sciex, Darmstadt,
554 Germany) ultrahigh performance liquid chromatography system. A multiple reaction
555 monitoring (MRM) method was used for the detection and quantification of the bile acids. An
556 electrospray ion voltage of −4500 V and the following ion source parameters were used: curtain

557 gas (35 psi), temperature (450 °C), gas 1 (55 psi), gas 2 (65 psi), and entrance potential (−10
558 V). The MS parameters and LC conditions were optimized using commercially available
559 standards of endogenous bile acids and deuterated bile acids, for the simultaneous
560 quantification of selected 28 analytes. For separation of the analytes a 100 × 2.1 mm, 100 Å,
561 1.7 µm, Kinetex C18 column (Phenomenex, Aschaffenburg, Germany) was used.
562 Chromatographic separation was performed with a constant flow rate of 0.4 mL/min using a
563 mobile phase consisted of water (eluent A) and acetonitrile/water (95/5, v/v, eluent B), both
564 containing 5 mM ammonium acetate and 0.1% formic acid. The gradient elution started with
565 25% B for 2 min, increased at 3.5 min to 27% B, in 2 min to 35% B, which was hold until 10
566 min, increased in 1 min to 43% B, held for 1 min, increased in 2 min to 58% B; held 3 min
567 isocratically at 58% B, then the concentration was increased to 65% at 17.5 min, with another
568 increase to 80% B at 18 min, following an increase at 19 min to 100% B which was hold for 1
569 min, at 20.5 min the column was equilibrated for 4.5 min at starting. The injection volume for
570 all samples was 1 µL, the column oven temperature was set to 40 °C, and the auto-sampler was
571 kept at 15 °C. Data acquisition and instrumental control were performed with Analyst 1.7
572 software (Sciex, Darmstadt, Germany) as previously described [90]. Briefly, a standard curve (0.5
573 nM to 15000 nM, 16 points), linear regression and weighting type of 1/x was used to calculated
574 BA concentrations [90]. BAs measured are Cholic acid (CA), chenodeoxycholic acid (CDCA),
575 a-Muricholic acid (aMCA), b-Muricholic acid (bMCA), Taurocholic acid (TCA),
576 Taurochenodeoxycholic acid (TCDCA), Tauroursodeoxycholic acid (TUDCA),
577 Taurohyodeoxycholic acid (THDCA), Taurolithocholic acid (TLCA), Taurodeoxycholic acid
578 (TDCA), Tauro-a-Muricholic acid (TaMCA), Glycochenodeoxycholic acid (GCDCA),
579 Glycocholic acid (GCA), Deoxycholic acid (DCA), Lithocholic acid (LCA), y-Muricholic acid
580 (y-MCA), 12-Dehydrocholic acid (12-DHCA), 12-Ketolithocholic acid (12-keto-LCA), 3-
581 Dehydrocholic acid (3-DHCA), 6-Ketolithocholic acid (6-keto-LCA), 7-Dehydrocholic acid (7-
582 DHCA), 7-Sulfocholic acid (7-sulfo-CA), Allocholic acid (ACA), Cholic acid-7ol-3one (CA-

583 7ol-3one), Ursocholic acid (UCA), Dehydrolithocholic acid (DHLCA), Hyodeoxycholic acid
584 (HDCA), Murideoxycholic acid (MDCA), Ursodeoxycholic acid (UDCA).

585 *Targeted short-chain fatty acid measurement*

586 For the quantitation of short-chain fatty acids (SCFAs) the 3-NPH method was used [91]. Briefly,
587 40 µL of the fecal extract and 15 µL of isotopically labeled standards (ca 50 µM) were mixed
588 with 20 µL 120 mM EDC HCl-6% pyridine-solution and 20 µL of 200 mM 3-NPH HCL
589 solution. After 30 min at 40°C and shaking at 1000 rpm using an Eppendorf Thermomix
590 (Eppendorf, Hamburg, Germany), 900 µL acetonitrile/water (50/50, v/v) was added. After
591 centrifugation at 13000 U/min for 2 min the clear supernatant was used for analysis. The same
592 system as described above was used. The electrospray voltage was set to -4500 V, curtain gas
593 to 35 psi, ion source gas 1 to 55, ion source gas 2 to 65 and the temperature to 500°C. The
594 MRM-parameters were optimized using commercially available standards for the SCFAs. The
595 chromatographic separation was performed on a 100 × 2.1 mm, 100 Å, 1.7 µm, Kinetex C18
596 column (Phenomenex, Aschaffenburg, Germany) column with 0.1% formic acid (eluent A) and
597 0.1% formic acid in acetonitrile (eluent B) as elution solvents. An injection volume of 1 µL and
598 a flow rate of 0.4 mL/min was used. The gradient elution started at 23% B which was held for
599 3 min, afterward the concentration was increased to 30% B at 4 min, with another increase to
600 40%B at 6.5 min, at 7 min 100% B was used which was hold for 1 min, at 8.5 min the column
601 was equilibrated at starting conditions. The column oven was set to 40°C and the autosampler
602 to 15°C. Data acquisition and instrumental control were performed with Analyst 1.7 software
603 (Sciex, Darmstadt, Germany). Concentrations of SCFA were calculated with the use of linear
604 regression using a standard curve (ranging 0.0004 mM to 2 mM (12 points), SCFAs measured
605 are Acetate, Propionate, Butyrate, Valeric acid, Desaminotyrosine and the Branched-chain
606 Fatty acids (Isobutyric acid, 2-Methylbutyric acid and Isovaleric acid).

607 *Targeted metabolite analyses*

608 MultiQuant 3.0.3 Software (AB Sciex) was used to integrate the data and calculate the
609 concentration. Isotopically labelled standards were used for SCFA quantitation. For bile acid
610 quantitation, we used Dehydrocholic acid as internal standard to correct for losses during
611 sample preparation and isotopically labelled references to correct for ionization effects during
612 measurement, according to the paper of Sinah et al. 2021 [90]. For comparison between two
613 groups, Mann-Whitney U test was used to test for statistical significance. Metabolite-
614 microbiota correlation analyses was performed on relative abundance zOTU level within the
615 rhythmic in male *Bmal1*$^{fl/fl}$, but not *Bmal1*$^{IEC-/-}$ samples with at least a 30% prevalence.
616 Spearman correlation and adjusted p-values between targeted metabolomics and zOTUs were
617 calculated using the *rcor()* function in R. Correlation matrixes were visualized within the R
618 package "corrplot" (Wei et al., 2017). Only correlations were plotted with a P-value of <0.05
619 and coefficient values $R \leq -0.5$ and ≥ 0.5. Furthermore, M2IA online platform [92] was used for
620 the global similarity analyses (PA plot) between metabolome and microbiota data.

621 *Transfer experiments*

622 Mice were gavaged with cecal microbiota at ZT13 from either cecal content (CT/ZT13) of
623 *Bmal1*$^{IEC-/-}$ mice (n=4, mixture), or control mice kept in LD (n=5, mixture), DD (n=4) or
624 starvation (n=5) into germ-free wild type C57BL6 recipient mice. 100µl of $7x10^6$ bacteria/µl
625 were used for gavaging each mouse. Mice were weekly monitored for bodyweight changes and
626 feces was sampled at week 5 after gavage in DNA stabilizer. Afterwards, mice were sacrificed
627 at the 2nd day in DD at CT13. Native fecal samples for targeted metabolomics were taken at
628 ZT4 and ZT16.

629 *Immune cell isolation from the lamina propria*

630 Immune cells were isolated from freshly isolated jejunum and colon. Intestinal tissues were
631 flipped, washed out and cut into 1 cm pieces. To remove epithelial cells, pieces were incubated

632 in DMEM with 20 µL of 1M DTT. After shaking for 15 minutes, tissues were incubated PBS
633 with 200 µL of 150mM EDTA at 37°C with shaking. After 3 times harsh shaking in Hanks
634 buffer, jejunum tissue was then digested at 37°C for approximately 15 min in Thermoshake
635 (200rpm) with 0.6 mg/ml type VIII collagenase (Sigma-Aldrich). Colonic tissue was
636 simultaneously digested under the same condition for approximately 25 min but with the
637 mixture of 0.85 mg/ml type V collagenase (Sigma-Aldrich), 1.25 mg/ml collagenase D (Sigma-
638 Aldrich), 10µl/ml Amphotericin (100x) 1 mg/mL Dispase II, and 30U/ml Deoxyribonuclease I
639 (Sigma). Following digestion, intestinal cells were passed through a 40 µm strainer.
640 Consequently, cells were fixed with 2% PFA, washed, and stored in RPMI at 4 °C until further
641 processing.

642 *Fluorescence-activated cell sorting (FACS)*

643 For intracellular stainings, cells were permeabilized with saponin 0.5% and stained with anti
644 CD8 PE-, anti CD3 PerCP/Cy5.5, anti CD4 FITC-, anti IL-17a PE/cy7-, anti INFy- APC
645 conjugated antibodies at dilution 1/100-1/50 for 30 min.

646 Surface stainings were performed using anti CD11c PE-, anti CD11b APC Cy7-, anti F4/80
647 PE/cy7-, anti Ly6G APC conjugated antibodies at dilution 1/50 for 30 minutes. Cells were
648 analyzed on a LSR-II (BD Biosciences) flow cytometer and analysis was performed using
649 FlowJo software (FlowJo, LLC).

650 *Histology*

651 In formalin fixated tissues in paraffine were cut into 5 µm thick slices and consequently stained
652 according to the following steps: xylene/ 5 min, xylene/ 5 min, Ethanol 100%/ 5 min, Ethanol
653 100%/ 5 min, Ethanol 96%/ 2 min, Ethanol 96%/ 2 min, Ethanol 70%/ 2 min, Ethanol 70%/ 2
654 min, Water/ 30 s, hematoxylin/ 2 min, tap water/ 15 s, Scotts Tap Water/ 30 s, Water/ 30 s,
655 Ethanol 96%/ 30 s, Eosin/ 30 s, Ethanol 96%/ 30s, Ethanol 96%/ 30 s, Ethanol 100%/ 30 s,
656 Ethanol 100%/ 30 s, Xylene/ 90 s, Xylene/ 90s (Leica ST5020 multistainer). DPX new

657 mounting media (Merck) was added to preserve the tissues. Stained slides were scanned and
658 further analyzed for histological scoring. Histological scores were assessed blindly based on
659 the degree of immune cell infiltration of all colonic wall layers (mucosa, submucosa and
660 muscularis), crypt hyperplasia, goblet cell depletion and mucosal damage, resulting in a score
661 from 0 (not inflamed) to 12 (severely inflamed) according to Katakura method [93].

662 *Immunofluorescence staining of CD3*

663 Antigens retrieval of the de-paraffinized and re-hydrated sections was performed by heating the
664 slices in citrate buffer for 34 minutes. After multiple washing steps and tissues were blocked
665 by donkey blocking buffer (1h at room temperature and 1hour at 4C). Tissue sections were
666 incubated overnight with Anti E-cadherin (1:300, mouse, Abcam) anti-CD3 (1:400, rabbit,
667 sigma). Tissue were washed with PBS and followed by incubation with secondary antibodies
668 (donkey anti rabbit 546, donkey anti mouse 647, both from invitrogen with a dilution 1:200)
669 for 1h at room temperature. Finally, DAPI (Sigma) were used to stain the nuclei and then
670 tissues were mounted using Aquatex. Sections were visualized with Fluoview FV10i
671 microscope (Olympus, Shinjuku, Japan).

672 *PICRUST 2.0*

673 For prediction of functional of metagenomic functionality. Sequence of the gut controlled
674 zOTUs, captured as described above, were used to construct the metagenome using
675 PICRUST2.0 [94]. Corrected zOTU 16s rRNA gene copy number is multiplied by the predicted
676 functionality to predicted the metagenome. Resulted enzymatic genes classified according to
677 Enzyme Commission (EC) numbers were mapped to Metacyc pathways. Superclasses were
678 removed and Metacyc pathways abundance was used for statistical analysis using STAMP
679 (2.1.3). Statistical differences were calculated based on White's non-parametric t-test and
680 Benjamini Hochberg dales discovery rate to adjusted for multiple testing.

Statistical Analyses

Statistical analyses were preformed using GraphPad Prism, version 9.0.0 (GraphPad Software), JTK_cycle v3.1.R ([25]) or R. With the use of the pipeline Rhea (Lagkouvardos) between-sample microbiota diversity is calculated by generalized UniFrac using GUniFrac v1.1. distances. Quantification of GUniFrac distances was always done in comparison to ZT1 or CT1. Circadian and diurnal patterns of individual 24h period graphs as well as phase calculation were analysed by fitting a cosine-wave equation: y=baseline+(amplitude·cos(2·π·((x-[phase shift)/24))), with a fixed 24-h period for phyla, richness and single zOTU or by using the non-parametric algorithm JTK_cycle for overall rhythmicity of all zOTUs. Connected straight lines in of individual 24h period graphs within the figures indicate significant rhythmicity based on cosine analyses whereas dashed lines indicate non-significant cosine fit. Comparison of rhythm between data sets were preformed using an adjusted version of the Compare rhythm script [26], which performs JTK_cycle followed by DODR [95]. Some CCGs when indicated were analysed with a harmonic - regression: y= baseline + (amplitude A * cos (2·π· ((x - [phaseshift A) / 24))) + (amplitude B * cos (4·π·((x - [phase shift B) / 24))). Amplitude calculations depicted in the manhattan plots are based on the output of JTK_cycle and the phase was calculated by cosine-wave regression. Analysis between two groups was performed using the non-parametric Mann-Whitney test. A p value ≤0.05 was assumed as statistically significant.

Heatmaps were generated using the online tool "heatmapper.ca" [96]. Heatmaps were sorted based on peak phase of controls. Abundance plots were generated using SIAMCAT package in R using the "check.associations() function" [97]. Visualisation of zOTUs and samples trees were conducted using the online platform "evolgenius.info" [89].

Data availability

Microbiota sequencing data and metabolite data will be available from the Sequence Read Archive (SRA) and the MetaboLights database for Metabolomics experiments

(https://www.ebi.ac.uk/metabolights/) upon request. The modified version of the compare rhythm script is availabe (https://github.com) upon request.

References

1 Dunlap, J. C. Molecular bases for circadian clocks. *Cell* **96**, 271-290, doi:S0092-8674(00)80566-8 [pii] (1999).

2 Schibler, U., Ripperger, J. & Brown, S. A. Peripheral circadian oscillators in mammals: time and food. *J Biol Rhythms* **18**, 250-260, doi:10.1177/0748730403018003007 (2003).

3 Duguay, D. & Cermakian, N. The crosstalk between physiology and circadian clock proteins. *Chronobiol Int* **26**, 1479-1513, doi:10.3109/07420520903497575 (2009).

4 Zhang, R., Lahens, N. F., Ballance, H. I., Hughes, M. E. & Hogenesch, J. B. A circadian gene expression atlas in mammals: implications for biology and medicine. *Proc Natl Acad Sci U S A* **111**, 16219-16224, doi:10.1073/pnas.1408886111 (2014).

5 Pacha, J. & Sumova, A. Circadian regulation of epithelial functions in the intestine. *Acta Physiol (Oxf)* **208**, 11-24, doi:10.1111/apha.12090 (2013).

6 Hoogerwerf, W. A. Role of clock genes in gastrointestinal motility. *Am J Physiol Gastrointest Liver Physiol* **299**, G549-555, doi:10.1152/ajpgi.00147.2010 (2010).

7 Peterson, L. W. & Artis, D. Intestinal epithelial cells: regulators of barrier function and immune homeostasis. *Nat Rev Immunol* **14**, 141-153, doi:10.1038/nri3608 (2014).

8 Segers, A. & Depoortere, I. Circadian clocks in the digestive system. *Nat Rev Gastroenterol Hepatol* **18**, 239-251, doi:10.1038/s41575-020-00401-5 (2021).

9 Leone, V. *et al.* Effects of diurnal variation of gut microbes and high-fat feeding on host circadian clock function and metabolism. *Cell Host Microbe* **17**, 681-689, doi:10.1016/j.chom.2015.03.006 (2015).

10 Thaiss, C. A. *et al.* Transkingdom control of microbiota diurnal oscillations promotes metabolic homeostasis. *Cell* **159**, 514-529, doi:10.1016/j.cell.2014.09.048 (2014).

11 Zarrinpar, A., Chaix, A., Yooseph, S. & Panda, S. Diet and feeding pattern affect the diurnal dynamics of the gut microbiome. *Cell Metab* **20**, 1006-1017, doi:10.1016/j.cmet.2014.11.008 (2014).

12 Reitmeier, S. *et al.* Arrhythmic Gut Microbiome Signatures Predict Risk of Type 2 Diabetes. *Cell Host Microbe* **28**, 258-272 e256, doi:10.1016/j.chom.2020.06.004 (2020).

13 Liang, X., Bushman, F. D. & FitzGerald, G. A. Rhythmicity of the intestinal microbiota is regulated by gender and the host circadian clock. *Proc Natl Acad Sci U S A* **112**, 10479-10484, doi:10.1073/pnas.1501305112 (2015).

14 Voigt, R. M. *et al.* The Circadian Clock Mutation Promotes Intestinal Dysbiosis. *Alcohol Clin Exp Res* **40**, 335-347, doi:10.1111/acer.12943 (2016).

15 Coleman, O. I. *et al.* Activated ATF6 Induces Intestinal Dysbiosis and Innate Immune Response to Promote Colorectal Tumorigenesis. *Gastroenterology* **155**, 1539-1552 e1512, doi:10.1053/j.gastro.2018.07.028 (2018).

16 Lloyd-Price, J. *et al.* Multi-omics of the gut microbial ecosystem in inflammatory bowel diseases. *Nature* **569**, 655-662, doi:10.1038/s41586-019-1237-9 (2019).

17 Turnbaugh, P. J. *et al.* An obesity-associated gut microbiome with increased capacity for energy harvest. *Nature* **444**, 1027-1031, doi:10.1038/nature05414 (2006).

18 Ferraz-Bannitz, R. *et al.* Circadian Misalignment Induced by Chronic Night Shift Work Promotes Endoplasmic Reticulum Stress Activation Impacting Directly on Human Metabolism. *Biology (Basel)* **10**, doi:10.3390/biology10030197 (2021).

19 Gutierrez Lopez, D. E., Lashinger, L. M., Weinstock, G. M. & Bray, M. S. Circadian rhythms and the gut microbiome synchronize the host's metabolic response to diet. *Cell Metab*, doi:10.1016/j.cmet.2021.03.015 (2021).

20 Onaolapo, A. Y. & Onaolapo, O. J. Circadian dysrhythmia-linked diabetes mellitus: Examining melatonin's roles in prophylaxis and management. *World J Diabetes* **9**, 99-114, doi:10.4239/wjd.v9.i7.99 (2018).
21 Voigt, R. M. *et al.* Circadian disorganization alters intestinal microbiota. *PLoS One* **9**, e97500, doi:10.1371/journal.pone.0097500 (2014).
22 Aschoff, J. Exogenous and endogenous components in circadian rhythms. *Cold Spring Harb Symp Quant Biol* **25**, 11-28, doi:10.1101/sqb.1960.025.01.004 (1960).
23 Tourlousse, D. M. *et al.* Synthetic spike-in standards for high-throughput 16S rRNA gene amplicon sequencing. *Nucleic Acids Res* **45**, e23, doi:10.1093/nar/gkw984 (2017).
24 Thaiss, C. A. *et al.* Microbiota Diurnal Rhythmicity Programs Host Transcriptome Oscillations. *Cell* **167**, 1495-1510 e1412, doi:10.1016/j.cell.2016.11.003 (2016).
25 Hughes, M. E., Hogenesch, J. B. & Kornacker, K. JTK_CYCLE: an efficient nonparametric algorithm for detecting rhythmic components in genome-scale data sets. *J Biol Rhythms* **25**, 372-380, doi:10.1177/0748730410379711 (2010).
26 Pelikan, A., Herzel, H., Kramer, A. & Ananthasubramaniam, B. Venn diagram analysis overestimates the extent of circadian rhythm reprogramming. *FEBS J*, doi:10.1111/febs.16095 (2021).
27 Thaben, P. F. & Westermark, P. O. Differential rhythmicity: detecting altered rhythmicity in biological data. *Bioinformatics* **32**, 2800-2808, doi:10.1093/bioinformatics/btw309 (2016).
28 Damiola, F. *et al.* Restricted feeding uncouples circadian oscillators in peripheral tissues from the central pacemaker in the suprachiasmatic nucleus. *Genes Dev* **14**, 2950-2961, doi:10.1101/gad.183500 (2000).
29 Coleman, O. I. & Haller, D. Bacterial Signaling at the Intestinal Epithelial Interface in Inflammation and Cancer. *Front Immunol* **8**, 1927, doi:10.3389/fimmu.2017.01927 (2017).
30 Wu, M. *et al.* The Dynamic Changes of Gut Microbiota in Muc2 Deficient Mice. *Int J Mol Sci* **19**, doi:10.3390/ijms19092809 (2018).
31 Forman, R. A. *et al.* The goblet cell is the cellular source of the anti-microbial angiogenin 4 in the large intestine post Trichuris muris infection. *PLoS One* **7**, e42248, doi:10.1371/journal.pone.0042248 (2012).
32 Mukherji, A., Kobiita, A., Ye, T. & Chambon, P. Homeostasis in intestinal epithelium is orchestrated by the circadian clock and microbiota cues transduced by TLRs. *Cell* **153**, 812-827, doi:10.1016/j.cell.2013.04.020 (2013).
33 Kuang, Z. *et al.* The intestinal microbiota programs diurnal rhythms in host metabolism through histone deacetylase 3. *Science* **365**, 1428-1434, doi:10.1126/science.aaw3134 (2019).
34 Wang, Y. *et al.* The intestinal microbiota regulates body composition through NFIL3 and the circadian clock. *Science* **357**, 912-916, doi:10.1126/science.aan0677 (2017).
35 Hardbower, D. M. *et al.* Arginase 2 deletion leads to enhanced M1 macrophage activation and upregulated polyamine metabolism in response to Helicobacter pylori infection. *Amino Acids* **48**, 2375-2388, doi:10.1007/s00726-016-2231-2 (2016).
36 Biddle, A., Stewart, L., Blanchard, J. & Leschine, S. Untangling the Genetic Basis of Fibrolytic Specialization by Lachnospiraceae and Ruminococcaceae in Diverse Gut Communities. *Diversity* **5**, 627-640 (2013).
37 Ridlon, J. M., Kang, D. J., Hylemon, P. B. & Bajaj, J. S. Bile acids and the gut microbiome. *Current opinion in gastroenterology* **30**, 332-338, doi:10.1097/MOG.0000000000000057 (2014).
38 Ericsson, A. C., Personett, A. R., Turner, G., Dorfmeyer, R. A. & Franklin, C. L. Variable Colonization after Reciprocal Fecal Microbiota Transfer between Mice with Low and High Richness Microbiota. *Front Microbiol* **8**, 196, doi:10.3389/fmicb.2017.00196 (2017).
39 Gundersen, M. D. *et al.* Loss of interleukin 33 expression in colonic crypts - a potential marker for disease remission in ulcerative colitis. *Sci Rep* **6**, 35403, doi:10.1038/srep35403 (2016).
40 Liu, T., Zhang, L., Joo, D. & Sun, S. C. NF-kappaB signaling in inflammation. *Signal Transduct Target Ther* **2**, doi:10.1038/sigtrans.2017.23 (2017).
41 Hooper, L. V., Stappenbeck, T. S., Hong, C. V. & Gordon, J. I. Angiogenins: a new class of microbicidal proteins involved in innate immunity. *Nat Immunol* **4**, 269-273, doi:10.1038/ni888 (2003).

42 Mardinoglu, A. *et al.* The gut microbiota modulates host amino acid and glutathione metabolism in mice. *Mol Syst Biol* **11**, 834, doi:10.15252/msb.20156487 (2015).
43 Wu, G. *et al.* Light exposure influences the diurnal oscillation of gut microbiota in mice. *Biochem Biophys Res Commun* (2018).
44 Deaver, J. A., Eum, S. Y. & Toborek, M. Circadian Disruption Changes Gut Microbiome Taxa and Functional Gene Composition. *Front Microbiol* **9**, 737, doi:10.3389/fmicb.2018.00737 (2018).
45 Edgar, R. C. Updating the 97% identity threshold for 16S ribosomal RNA OTUs. *Bioinformatics* **34**, 2371-2375, doi:10.1093/bioinformatics/bty113 (2018).
46 Frazier, K. *et al.* High fat diet disrupts diurnal interactions between REG3g and small intestinal gut microbes resulting in metabolic dysfunction. *bioRxiv* (2020).
47 Alenghat, T. *et al.* Histone deacetylase 3 coordinates commensal-bacteria-dependent intestinal homeostasis. *Nature* **504**, 153-157, doi:10.1038/nature12687 (2013).
48 Caricilli, A. M. *et al.* Gut microbiota is a key modulator of insulin resistance in TLR 2 knockout mice. *PLoS Biol* **9**, e1001212, doi:10.1371/journal.pbio.1001212 (2011).
49 Wu, S. E. *et al.* Microbiota-derived metabolite promotes HDAC3 activity in the gut. *Nature* **586**, 108-112, doi:10.1038/s41586-020-2604-2 (2020).
50 Schroeder, B. O. Fight them or feed them: how the intestinal mucus layer manages the gut microbiota. *Gastroenterol Rep (Oxf)* **7**, 3-12, doi:10.1093/gastro/goy052 (2019).
51 Bishehsari, F., Voigt, R. M. & Keshavarzian, A. Circadian rhythms and the gut microbiota: from the metabolic syndrome to cancer. *Nat Rev Endocrinol* **16**, 731-739, doi:10.1038/s41574-020-00427-4 (2020).
52 Tailford, L. E., Crost, E. H., Kavanaugh, D. & Juge, N. Mucin glycan foraging in the human gut microbiome. *Front Genet* **6**, 81, doi:10.3389/fgene.2015.00081 (2015).
53 Carr, F. J., Chill, D. & Maida, N. The lactic acid bacteria: a literature survey. *Crit Rev Microbiol* **28**, 281-370, doi:10.1080/1040-840291046759 (2002).
54 Gerard, P. Metabolism of cholesterol and bile acids by the gut microbiota. *Pathogens* **3**, 14-24, doi:10.3390/pathogens3010014 (2013).
55 Beli, E., Prabakaran, S., Krishnan, P., Evans-Molina, C. & Grant, M. B. Loss of Diurnal Oscillatory Rhythms in Gut Microbiota Correlates with Changes in Circulating Metabolites in Type 2 Diabetic db/db Mice. *Nutrients* **11**, doi:10.3390/nu11102310 (2019).
56 Govindarajan, K. *et al.* Unconjugated Bile Acids Influence Expression of Circadian Genes: A Potential Mechanism for Microbe-Host Crosstalk. *PLoS One* **11**, e0167319, doi:10.1371/journal.pone.0167319 (2016).
57 Vavassori, P., Mencarelli, A., Renga, B., Distrutti, E. & Fiorucci, S. The bile acid receptor FXR is a modulator of intestinal innate immunity. *J Immunol* **183**, 6251-6261, doi:10.4049/jimmunol.0803978 (2009).
58 Kim, M. H., Kang, S. G., Park, J. H., Yanagisawa, M. & Kim, C. H. Short-chain fatty acids activate GPR41 and GPR43 on intestinal epithelial cells to promote inflammatory responses in mice. *Gastroenterology* **145**, 396-406 e391-310, doi:10.1053/j.gastro.2013.04.056 (2013).
59 Segers, A. *et al.* The circadian clock regulates the diurnal levels of microbial short-chain fatty acids and their rhythmic effects on colon contractility in mice. *Acta Physiol (Oxf)* **225**, e13193, doi:10.1111/apha.13193 (2019).
60 Bhutta, H. Y. *et al.* Effect of Roux-en-Y gastric bypass surgery on bile acid metabolism in normal and obese diabetic rats. *PLoS One* **10**, e0122273, doi:10.1371/journal.pone.0122273 (2015).
61 Haeusler, R. A., Astiarraga, B., Camastra, S., Accili, D. & Ferrannini, E. Human insulin resistance is associated with increased plasma levels of 12alpha-hydroxylated bile acids. *Diabetes* **62**, 4184-4191, doi:10.2337/db13-0639 (2013).
62 Brufau, G. *et al.* Improved glycemic control with colesevelam treatment in patients with type 2 diabetes is not directly associated with changes in bile acid metabolism. *Hepatology* **52**, 1455-1464, doi:10.1002/hep.23831 (2010).
63 Zheng, X. *et al.* Hyocholic acid species as novel biomarkers for metabolic disorders. *Nat Commun* **12**, 1487, doi:10.1038/s41467-021-21744-w (2021).
64 Yoshimoto, S. *et al.* Obesity-induced gut microbial metabolite promotes liver cancer through senescence secretome. *Nature* **499**, 97-101, doi:10.1038/nature12347 (2013).

65 Ozcan, U. *et al.* Chemical chaperones reduce ER stress and restore glucose homeostasis in a mouse model of type 2 diabetes. *Science* **313**, 1137-1140, doi:10.1126/science.1128294 (2006).
66 Kars, M. *et al.* Tauroursodeoxycholic Acid may improve liver and muscle but not adipose tissue insulin sensitivity in obese men and women. *Diabetes* **59**, 1899-1905, doi:10.2337/db10-0308 (2010).
67 Jia, W., Xie, G. & Jia, W. Bile acid-microbiota crosstalk in gastrointestinal inflammation and carcinogenesis. *Nat Rev Gastroenterol Hepatol* **15**, 111-128, doi:10.1038/nrgastro.2017.119 (2018).
68 Narimatsu, K. *et al.* Toll-like receptor (TLR) 2 agonists ameliorate indomethacin-induced murine ileitis by suppressing the TLR4 signaling. *J Gastroenterol Hepatol* **30**, 1610-1617, doi:10.1111/jgh.12980 (2015).
69 Maslowski, K. M. *et al.* Regulation of inflammatory responses by gut microbiota and chemoattractant receptor GPR43. *Nature* **461**, 1282-1286, doi:10.1038/nature08530 (2009).
70 Barker, N. *et al.* Identification of stem cells in small intestine and colon by marker gene Lgr5. *Nature* **449**, 1003-1007, doi:10.1038/nature06196 (2007).
71 Bamias, G. *et al.* Intestinal-specific TNFalpha overexpression induces Crohn's-like ileitis in mice. *PLoS One* **8**, e72594, doi:10.1371/journal.pone.0072594 (2013).
72 Rakoff-Nahoum, S., Paglino, J., Eslami-Varzaneh, F., Edberg, S. & Medzhitov, R. Recognition of commensal microflora by toll-like receptors is required for intestinal homeostasis. *Cell* **118**, 229-241, doi:10.1016/j.cell.2004.07.002 (2004).
73 Valentini, M. *et al.* Immunomodulation by gut microbiota: role of Toll-like receptor expressed by T cells. *J Immunol Res* **2014**, 586939, doi:10.1155/2014/586939 (2014).
74 Xiao, Y. *et al.* Interleukin-33 Promotes REG3gamma Expression in Intestinal Epithelial Cells and Regulates Gut Microbiota. *Cell Mol Gastroenterol Hepatol* **8**, 21-36, doi:10.1016/j.jcmgh.2019.02.006 (2019).
75 Dou, X. *et al.* TLR2/4-mediated NF-kappaB pathway combined with the histone modification regulates beta-defensins and interleukins expression by sodium phenyl butyrate in porcine intestinal epithelial cells. *Food Nutr Res* **62**, doi:10.29219/fnr.v62.1493 (2018).
76 Zheng, D., Liwinski, T. & Elinav, E. Interaction between microbiota and immunity in health and disease. *Cell Res* **30**, 492-506, doi:10.1038/s41422-020-0332-7 (2020).
77 Metwaly, A. *et al.* Integrated microbiota and metabolite profiles link Crohn's disease to sulfur metabolism. *Nat Commun* **11**, 4322, doi:10.1038/s41467-020-17956-1 (2020).
78 Kawai, M. *et al.* Intestinal clock system regulates skeletal homeostasis. *JCI Insight* **4**, doi:10.1172/jci.insight.121798 (2019).
79 Ubeda, C. *et al.* Familial transmission rather than defective innate immunity shapes the distinct intestinal microbiota of TLR-deficient mice. *J Exp Med* **209**, 1445-1456, doi:10.1084/jem.20120504 (2012).
80 Jud, C., Schmutz, I., Hampp, G., Oster, H. & Albrecht, U. A guideline for analyzing circadian wheel-running behavior in rodents under different lighting conditions. *Biol Proced Online* **7**, 101-116, doi:10.1251/bpo109 (2005).
81 Li, Z. *et al.* Essential roles of enteric neuronal serotonin in gastrointestinal motility and the development/survival of enteric dopaminergic neurons. *J Neurosci* **31**, 8998-9009, doi:10.1523/JNEUROSCI.6684-10.2011 (2011).
82 Godon, J. J., Zumstein, E., Dabert, P., Habouzit, F. & Moletta, R. Molecular microbial diversity of an anaerobic digestor as determined by small-subunit rDNA sequence analysis. *Appl Environ Microbiol* **63**, 2802-2813, doi:10.1128/aem.63.7.2802-2813.1997 (1997).
83 Edgar, R. C. Search and clustering orders of magnitude faster than BLAST. *Bioinformatics* **26**, 2460-2461, doi:10.1093/bioinformatics/btq461 (2010).
84 Edgar, R. C., Haas, B. J., Clemente, J. C., Quince, C. & Knight, R. UCHIME improves sensitivity and speed of chimera detection. *Bioinformatics* **27**, 2194-2200, doi:10.1093/bioinformatics/btr381 (2011).
85 Edgar, R. C. UNOISE2: improved error-correction for Illumina 16S and ITS amplicon sequencing. *bioRxiv*, 081257, doi:10.1101/081257 (2016).

923 86 Yoon, S. H. *et al.* Introducing EzBioCloud: a taxonomically united database of 16S rRNA
924 gene sequences and whole-genome assemblies. *Int J Syst Evol Microbiol* **67**, 1613-1617,
925 doi:10.1099/ijsem.0.001755 (2017).
926 87 Lagkouvardos, I., Fischer, S., Kumar, N. & Clavel, T. Rhea: a transparent and modular R
927 pipeline for microbial profiling based on 16S rRNA gene amplicons. *PeerJ* **5**, e2836,
928 doi:10.7717/peerj.2836 (2017).
929 88 Kumar, S., Stecher, G., Li, M., Knyaz, C. & Tamura, K. MEGA X: Molecular Evolutionary
930 Genetics Analysis across Computing Platforms. *Mol Biol Evol* **35**, 1547-1549,
931 doi:10.1093/molbev/msy096 (2018).
932 89 Subramanian, B., Gao, S., Lercher, M. J., Hu, S. & Chen, W.-H. Evolview v3: a webserver for
933 visualization, annotation, and management of phylogenetic trees. *Nucleic Acids Research* **47**,
934 W270-W275, doi:10.1093/nar/gkz357 (2019).
935 90 Reiter, S. *et al.* Development of a Highly Sensitive Ultra-High-Performance Liquid
936 Chromatography Coupled to Electrospray Ionization Tandem Mass Spectrometry Quantitation
937 Method for Fecal Bile Acids and Application on Crohn's Disease Studies. *J Agric Food Chem*
938 **69**, 5238-5251, doi:10.1021/acs.jafc.1c00769 (2021).
939 91 Han, J., Lin, K., Sequeira, C. & Borchers, C. H. An isotope-labeled chemical derivatization
940 method for the quantitation of short-chain fatty acids in human feces by liquid
941 chromatography-tandem mass spectrometry. *Anal Chim Acta* **854**, 86-94,
942 doi:10.1016/j.aca.2014.11.015 (2015).
943 92 Ni, Y. *et al.* M2IA: a web server for microbiome and metabolome integrative analysis.
944 *Bioinformatics* **36**, 3493-3498, doi:10.1093/bioinformatics/btaa188 (2020).
945 93 Katakura, K. *et al.* Toll-like receptor 9-induced type I IFN protects mice from experimental
946 colitis. *J Clin Invest* **115**, 695-702, doi:10.1172/JCI22996 (2005).
947 94 Douglas, G. M. *et al.* PICRUSt2 for prediction of metagenome functions. *Nature*
948 *Biotechnology* **38**, 685-688, doi:10.1038/s41587-020-0548-6 (2020).
949 95 Singer, J. M. & Hughey, J. J. LimoRhyde: A Flexible Approach for Differential Analysis of
950 Rhythmic Transcriptome Data. *J Biol Rhythms* **34**, 5-18, doi:10.1177/0748730418813785
951 (2019).
952 96 Babicki, S. *et al.* Heatmapper: web-enabled heat mapping for all. *Nucleic Acids Res* **44**,
953 W147-153, doi:10.1093/nar/gkw419 (2016).
954 97 Wirbel, J. *et al.* Microbiome meta-analysis and cross-disease comparison enabled by the
955 SIAMCAT machine-learning toolbox. *bioRxiv*, 2020.2002.2006.931808,
956 doi:10.1101/2020.02.06.931808 (2020).

Figure 1

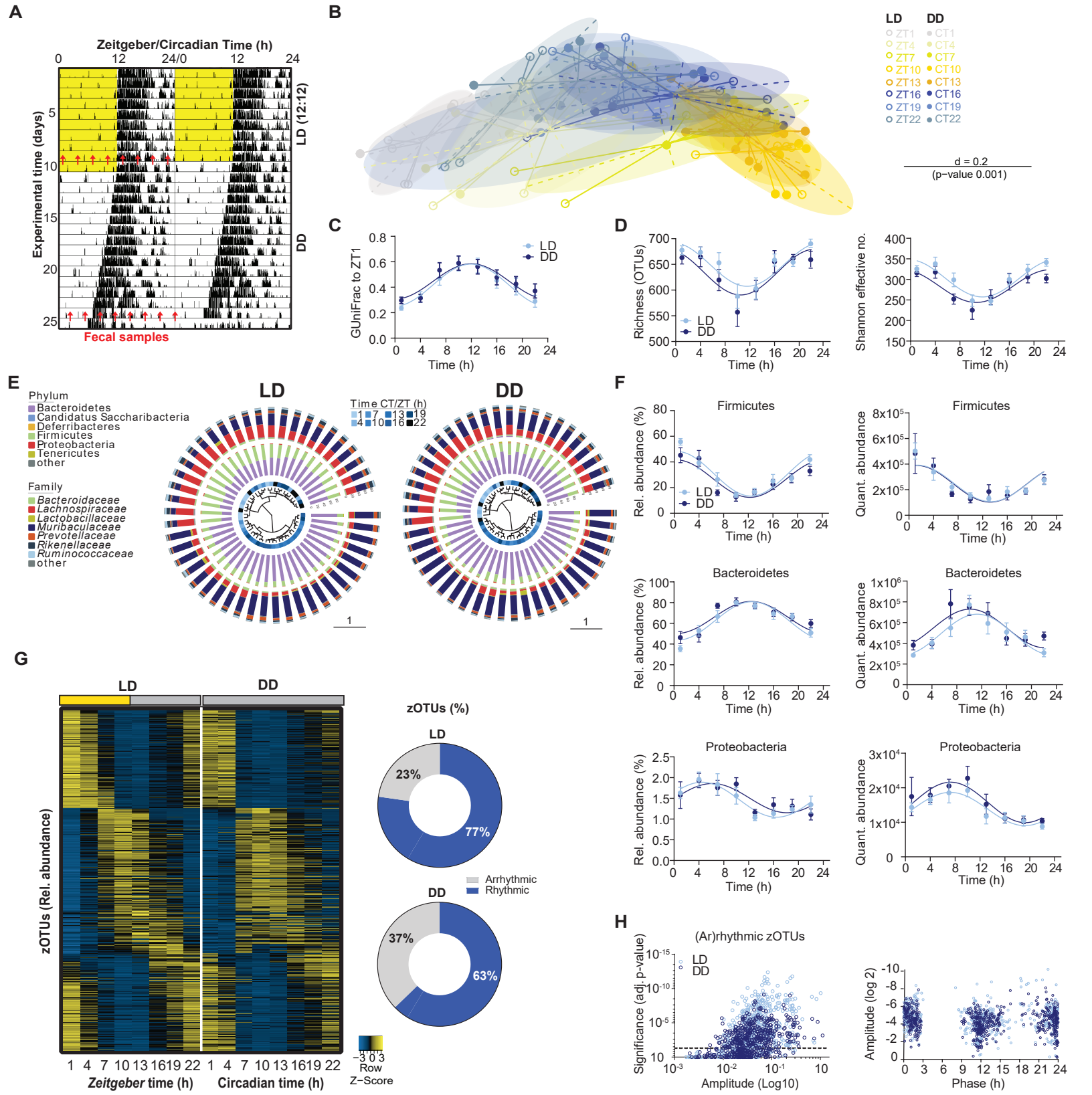

Figure 1 Fecal microbial rhythms persist in constant darkness (A) Representative actogram of control (*Bmal1*$^{IECfl/fl}$) mice exposed to light-dark (LD) cycle and two weeks of constant darkness (DD). Fecal sampling times are indicated by red arrows. (B) Beta-diversity principal coordinates analyses plot (PCoA) of fecal microbiota based on generalized UniFrac distances (GUniFrac) in LD and DD conditions and its quantification over time relative to ZT1 (C). (D) Diurnal (LD) and circadian (DD) profiles of alpha-diversity. (E) Dendrogram of microbiota profiles based on GUniFrac in LD and DD conditions. Taxonomic composition at phylum and family level for each sample is shown as stacked bar plots around the dendrogram. The blue inner circle indicates the sampling time. (F) Diurnal (LD) and circadian (DD) profiles of the relative (left) and quantitative abundance (right) of phyla. (G) Heatmap depicting the relative abundance of 580 zOTUs (mean relative abundance > 0.1%; prevalence > 10%). Data are normalized to the peak of each zOTU and ordered by the peak phase in LD conditions. Pie-charts at the right indicate the amount of rhythmic (blue) and arrhythmic (grey) zOTUs identified by JTK_Cycle (adj. p-value ≤ 0.05) (H) Significance and amplitude of rhythmic and arrhythmic zOTUs (left) and phase distribution (right) in LD and DD based on relative analysis. Significant rhythms are illustrated with fitted cosine-wave regression using a solid line (significance: p-value ≤ 0.05. LD (light-blue) and DD (dark-blue). n = 6 mice/time point/light condition. Data are represented as mean ± SEM.

Figure 2

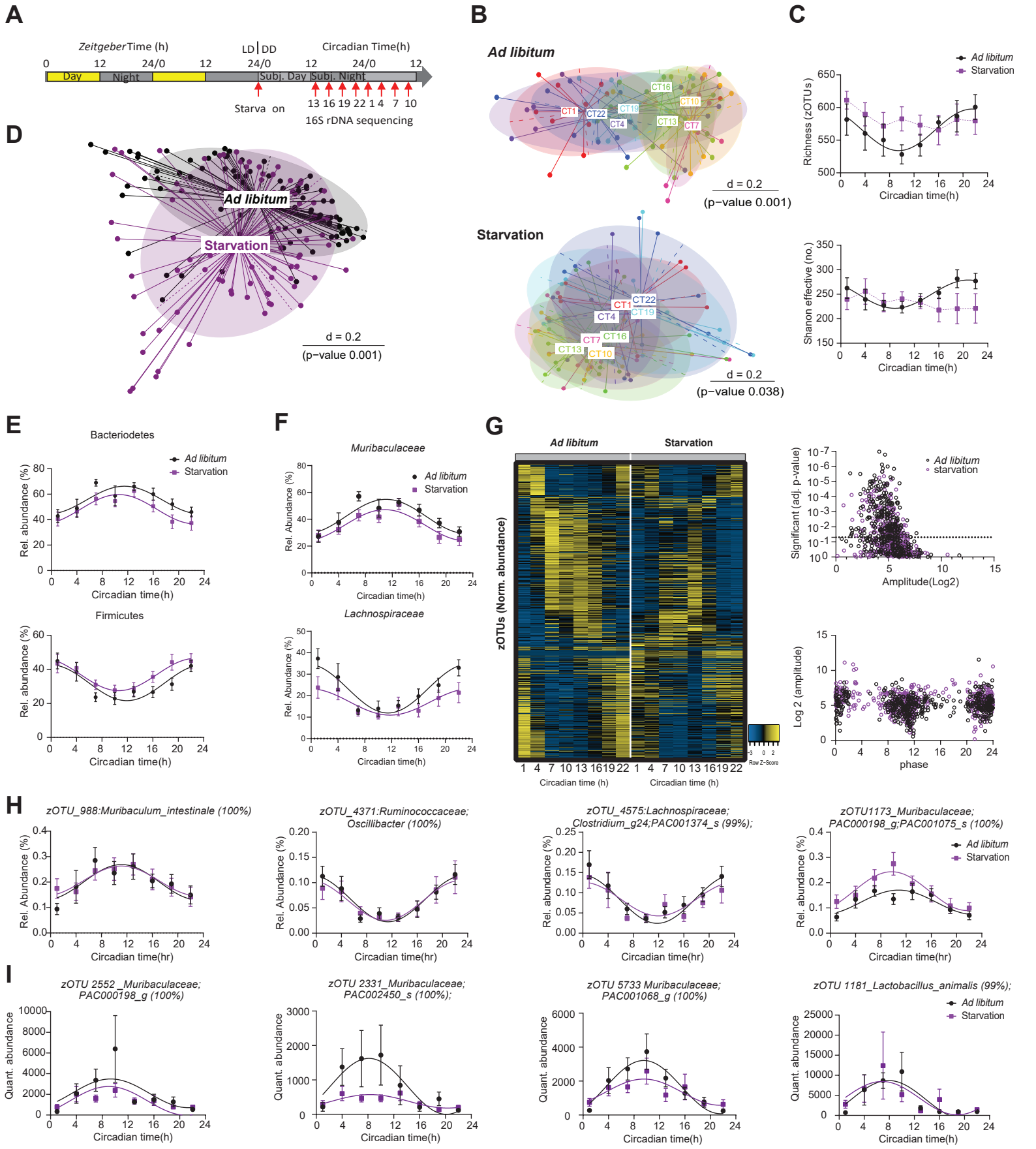

Figure 2 Food intake behavior marginally masks microbiota rhythmicity (A) Schematic illustration of the experiment design. (B) Beta-diversity principal coordinates analyses plots (PCoA) on generalized UniFrac distances (GUniFrac) distances of fecal microbiota stratified by individual time points in *ad libitum* (top) and starvation (buttom). (C) Circadian profiles of alpha-diversity. (D) PCoA plots of fecal microbiota based on GUniFrac distances stratified by feeding condition. (E, F) Circadian profiles of the relative abundance of the major phyla (E) and family (F) of fecal microbiota. (G) Heatmap depicting the relative abundance of 511 zOTUs (mean relative abundance > 0.1%; prevalence > 10%). Data are normalized to the peak of each zOTU and ordered by the peak phase in ad libitum condition. Significance and amplitude (JTK_Cycle analysis) of rhythmic and arrhythmic zOTUs (top) and phase distribution (based on cosine regression analysis) (bottom). Dashed line indicates adj p-value = 0.05. (H, I) Circadian profile of relative (H) and quantitative (I) abundance of zOTUs of fecal microbiota. Significant rhythms (cosine-wave regression, p-value ≤ 0.05) are illustrated with fitted cosine-wave curves; data points connected by dotted lines indicate no significant cosine fit curves (p-value > 0.05) and thus no rhythmicity. zOTUs were further analyzed with the adjusted compare rhythm script based on DODR. n = 9-11 mice/time point/light condition for relative data. n = 4-5 mice/time point/light condition for quantitative data. Data are represented by mean ± SEM.

Figure 3

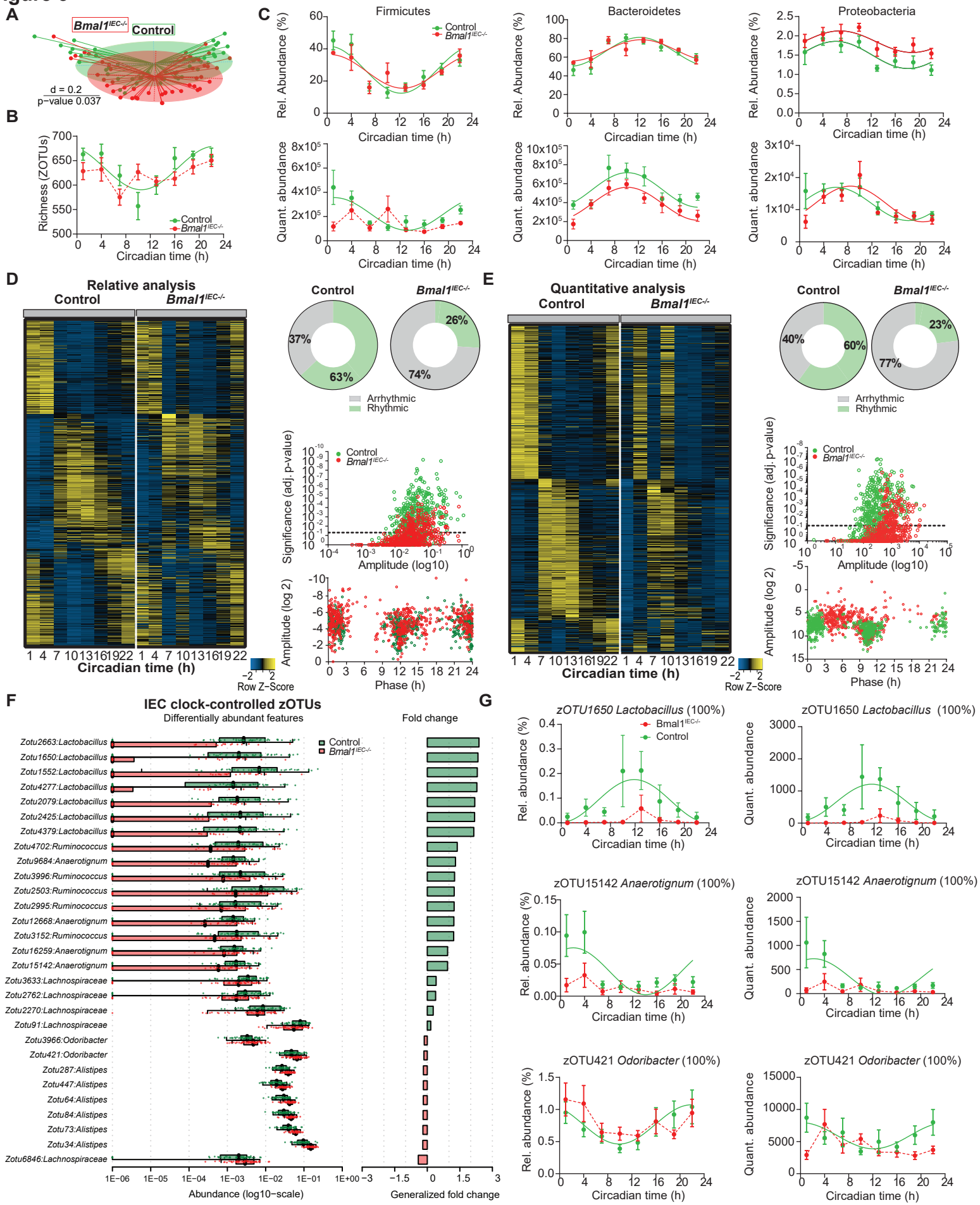

Figure 3 The intestinal circadian clock drives circadian microbiota composition (A) Beta-diversity principal coordinates analyses plot (PCoA) of fecal microbiota based on generalized UniFrac distances (GUniFrac) stratified by genotype. (B) Circadian profile of alpha diversity. (C) Circadian profile of relative (top) and quantitative (bottom) abundance of the major phyla. (D, E) Heatmap depicting the relative abundance (D) and quantitative abundance (E) of 580 zOTUs (mean relative abundance > 0.1%; prevalence > 10%). Data are normalized to the peak of each zOTU and ordered by the peak phase of control mice. Pie-charts at the right indicate the amount of rhythmic (colored) and arrhythmic (grey) zOTUs identified by JTK_Cycle (rhythmic = adj. p-value ≤ 0.05) based on relative (D) and quantitative (E) analysis. Significance and amplitude of rhythmic and arrhythmic zOTUs (top) and phase distribution (bottom) in controls and intestinal epithelial specific Bmal1-deficient (*Bmal1*$^{IEC-/-}$) mice is depicted on the right of the heatmaps. Dashed line indicates adj. p-value = 0.05 (JTK_Cycle). Bar charts in (F) represent the intestinal controlled zOTUs (adjusted compare rhythm script based on DODR) abundance comparison between control and *Bmal1*$^{IEC-/-}$(Wilcoxon, adj. p-value ≤ 0.05). Box and bar plots illustrate the alteration in quant. abundance (adj. p-value ≤ 0.05) and fold change of gut controlled zOTUs in the fecal samples with examples depicted in (G). Significant rhythms are illustrated with fitted cosine-regression solid lines; data points connected by dotted lines indicate no significant cosine fit curves (p-value > 0.05) and thus no rhythmicity. *Bmal1*$^{IECfl/fl}$ controls (green) and *Bmal1*$^{IEC-/-}$ (red). n = 5-6 mice/time point/genotype. Data are represented as mean ± SEM.

Figure 4

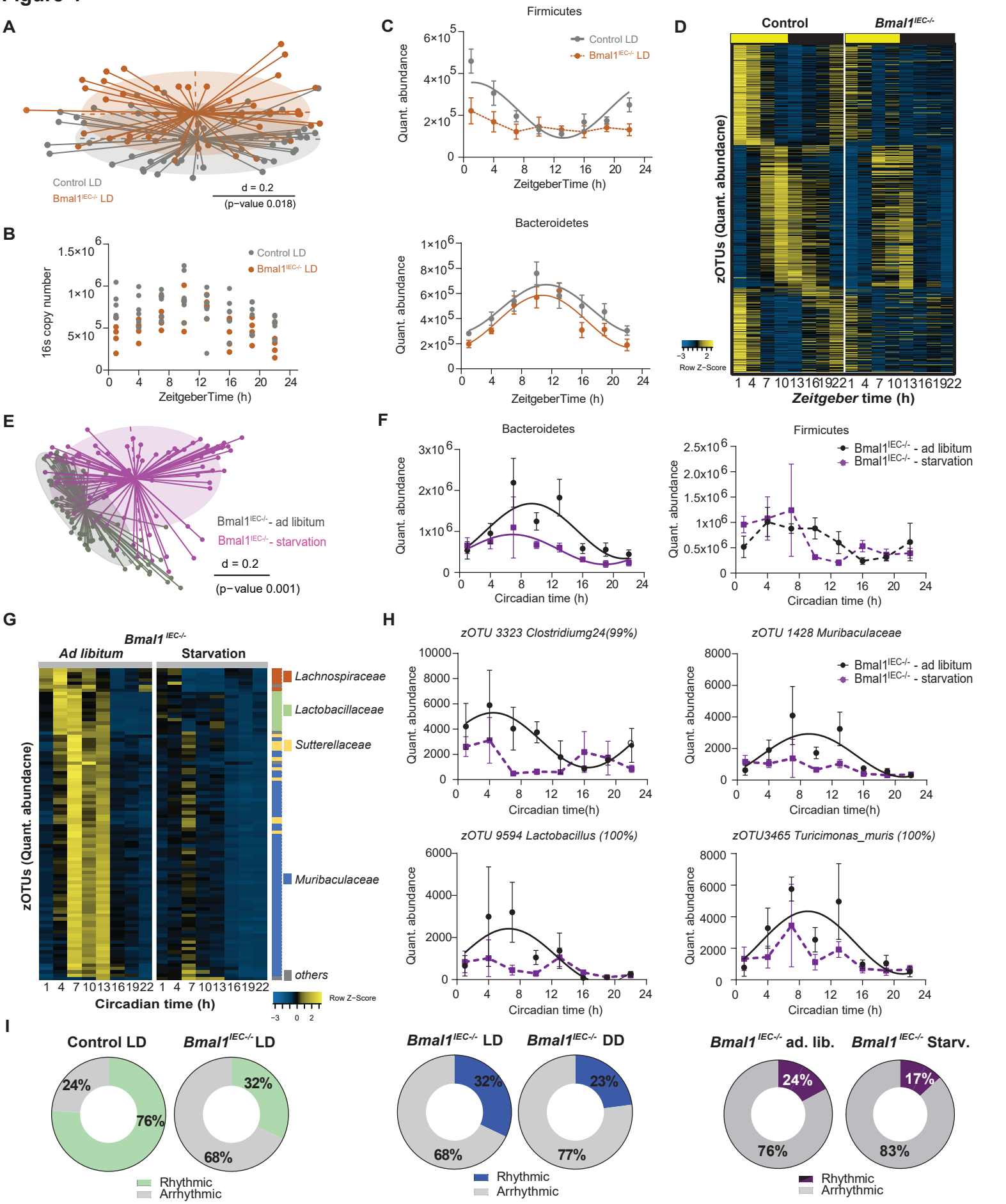

Figure 4 Microbiota profiling in *Bmal1*$^{IEC-/-}$ mice in LD conditions and under starvation (A) Beta-diversity principal coordinates analyses plot (PCoA) based on generalized UniFrac distances (GUniFrac) of fecal microbiota of *Bmal1*$^{IEC-/-}$ and their *Bmal1*$^{IECfl/fl}$ controls in LD conditons as well as the diurnal profiles of (B) 16s copy number (2-way ANOVA) and (C) major phyla quantitative abundance. (D) Heatmap illustrating zOTUs quantitative abundance over time of fecal microbiota of *Bmal1*$^{IEC-/-}$ and their controls in LD conditions. Data are ordered by the peak phase in LD conditions of the control group. (E) Beta-diversity principal coordinates analyses plot (PCoA) based on generalized UniFrac distances (GUniFrac) of fecal microbiota stratified by food availability. (F) Circadian profiles of phyla Firmicutes and Bacteroidetes. (G) Heatmap illustrating microbiota loosing/changing rhythmicity after starvation in *Bmal1*$^{IEC-/-}$ mice according to the adjusted compare rhythm script based on DODR (adj. p-value ≤ 0.05). Data are normalized to the peak of each zOTU and ordered by the peak phase in ad libitum condition. (H) Circadian profiles of the quantitative abundance of example zOTUs masked by the food-intake behavior (adjusted compare rhythm script based on DODR, adj. p-value ≤ 0.05). (I) Pie charts indicating the percentage of rhythmic/arrhythmic zOTUs in different condition according to JTK cycle analysis (rhythmic = adj. p-value ≤ 0.05). Significant rhythms (Cosine regression p-value ≤0.05) are illustrated with fitted cosine-regression; data points connected by dotted lines indicate no significant cosine fit curves (p-value > 0.05) and thus no rhythmicity. zOTUs were further analyzed with the adjusted compare rhythm script based on DODR. n = 3-6 mice/time point/condition. Data are represented as mean ± SEM

Figure 5

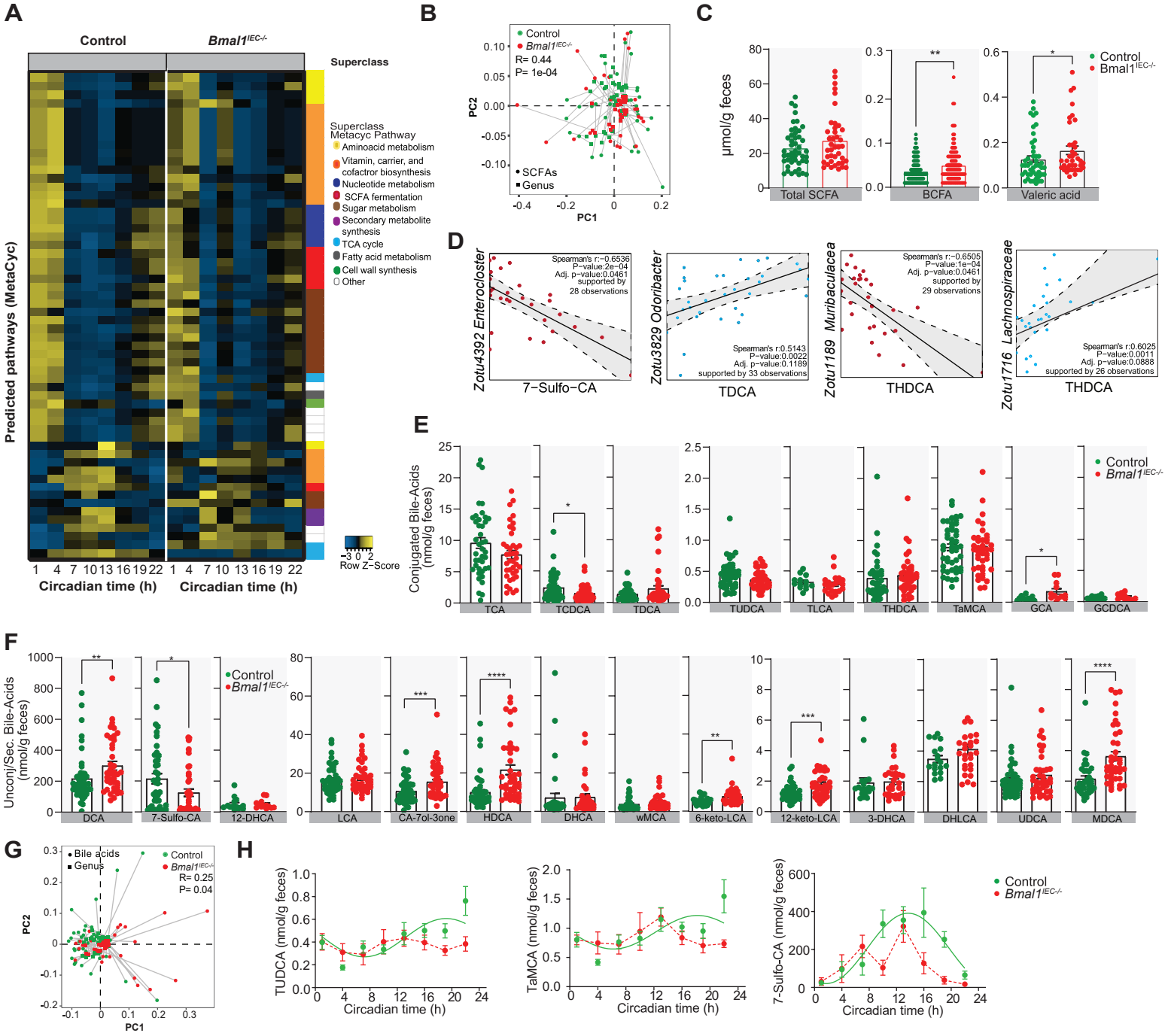

Figure 5 Metabolic functioning of intestinal clock-controlled bacteria (A) Heatmap of MetaCyc Pathways predicted using PICRUST2.0 on intestine clock-controlled zOTUs rhythmic in control (left) and arrhythmic in *Bmal1*$^{IEC-/-}$ (right) mice. Pathways are colored according to their sub-class. (B) Procrustes analyses (PA) of fecal microbiota and SCFA levels. The length of the line is proportional to the divergence between the data from the same mouse. (C) SCFA concentrations in feces. (D) and Spearman correlation (p-value ≤ 0.05 and R ≤ −0.5; red or R ≥ 0.5; blue) between SCFA and gut controlled bacteria taxa. (E) Conjugated and secondary (F) fecal BAs levels. (G) PA as described in (D) with fecal bile-acid (BA) levels. (H) Circadian profiles of BAs. Significant rhythms are illustrated with fitted cosine-regression (solid line); data points connected by dotted lines indicate no significant cosine fit curves (p-value > 0.05) and thus no rhythmicity. n = 5-6 mice/time point/genotype. Control (green) and *Bmal1*$^{IEC-/-}$ (red). Data are represented as mean ± SEM. Significance * p ≤ 0.05, ** p ≤ 0.01, *** p ≤ 0.001, **** p ≤ 0.0001 (Mann-Whitney U test). BCFA=branched-chain fatty acids. Cholic acid (CA), a-Muricholic acid (aMCA), b-Muricholic acid (bMCA), Taurocholic acid (TCA), Taurochenodeoxycholic acid (TCDCA), Tauroursodeoxycholic acid T(aTuUroDhCyAo)d,eoxycholic acid (THDCA), Taurolithocholic acid (TLCA), Taurodeoxycholic acid (TDCA), Tauro-a-Muricholic acid (TaMCA), Glycochenodeoxycholic a c(GidCDCA), Glycocholic acid (GCA), Deoxycholic acid (DCA), Lithocholic acid (LCA), y-Muricholic acid (y-MCA), 12-Dehydrocholic acid (12-DHCA), 12-Ketolithocholi cacid (12-ke-to-LCA), 3-Dehydrocholic acid (3-DHCA), 6-Ketolithocholic acid (6-keto-LCA), 7-Dehydrocholic acid (7-DHCA), 7-Sulfocholic acid (7-sulfo-CA), Allocho laiccid (ACA), Cholic acid-7ol-3one (CA-7ol-3one), Ursocholic acid (UCA), Dehydrolithocholic acid (DHLCA), Hyodeoxycholic acid (HDCA), Murideoxycholi c(MaDciCdA), Ursodeoxycholic acid (UDCA).

Figure 6

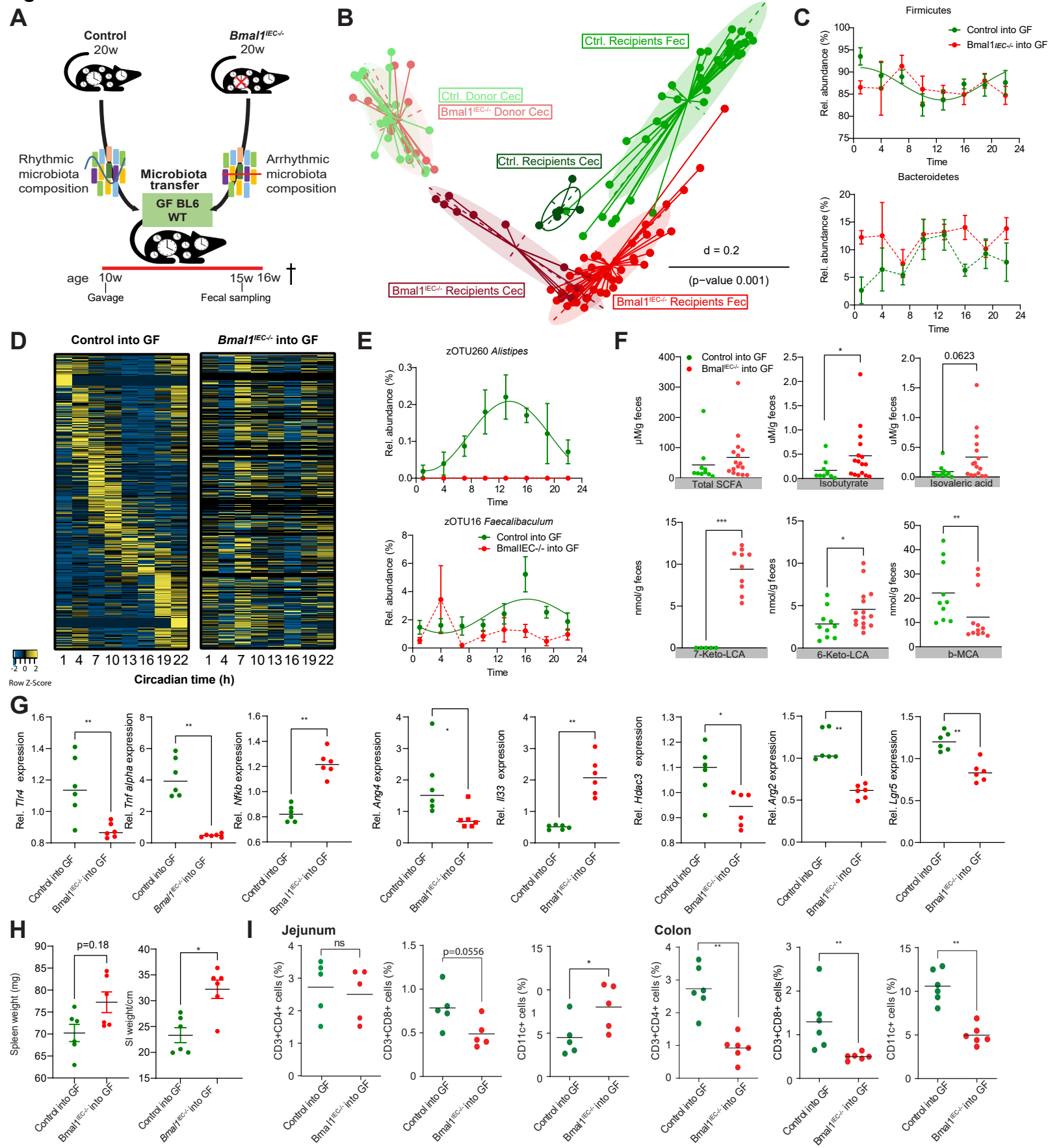

Figure 6 Intestinal clock-controlled rhythmic microbiota is essential for intestinal homeostasis (A) Schematic illustration of transfer experiments with mixture of cecal microbiota obtained from *Bmal1*$^{IECfl/fl}$ control and *Bmal1*$^{IEC-/-}$ donors (n=4) into 10 weeks old germ-free BL6 wild-type recipient mice till sacrifice at 16 weeks (16w). Fecal profiles were collected 5 weeks after gavage at the age of 15 weeks (15w). (B) PCoA plot of GUniFrac distances of donor (CT13) and recipient mice (n=6/genotype/time point) after 5 weeks of transfer. (C) Diurnal profiles of fecal microbiota at phylum level. (D) Heatmap depicting the relative abundance of zOTUs ordered by their cosine-regression peak phase according to the recipient controls. On the left the first two columns indicate donor zOTU abundance. (E) Diurnal profile of relative abundance of example zOTUs. (F) Fecal SCFA and BAs concentrations. (G) Relative gene expression of Tlr4, Arg2, Ang4, Tnfa, Il33, Nfkb, Hdac3, Lgr5 in the proximal colon of recipient mice. (H) Organ weights of recipient mice after receiving control (green) or *Bmal1*$^{IEC-/-}$ (red) cecal microbiota. (H) Frequency of CD3+CD4+, CD3+CD8+, CD11c+ cells in jejunum rhythms are illustrated with fitted cosine-regression; data points connected by dotted lines indicate no significant cosine fit curves (p-value > 0.05) and thus no rhythmicity. n = 6 mice/ genotype. Data are represented as mean ± SEM. Significance * $p \leq 0.05$, ** $p \leq 0.01$ (Mann-Whitney U test).